

# Spin-orbital resonating valence-bond liquid on a triangular lattice: Evidence from finite cluster diagonalization

Jiří Chaloupka

*Max-Planck-Institut für Festkörperforschung, Heisenbergstrasse 1, D-70569 Stuttgart, Germany and  
Department of Condensed Matter Physics, Faculty of Science,  
Masaryk University, Kotlářská 2, CZ-61137 Brno, Czech Republic*

Andrzej M. Oleś

*Max-Planck-Institut für Festkörperforschung, Heisenbergstrasse 1, D-70569 Stuttgart, Germany and  
Marian Smoluchowski Institute of Physics, Jagellonian University, Reymonta 4, PL-30059 Kraków, Poland  
(Dated: 16 December 2010)*

We investigate the ground state of the  $d^1$  spin-orbital model for triply degenerate  $t_{2g}$  orbitals on a triangular lattice which unifies intrinsic frustration of spin and orbital interactions with geometrical frustration. Using full or Lanczos exact diagonalization of finite clusters we establish that the ground state of the spin-orbital model which interpolates between the superexchange and direct exchange interactions on the bonds is characterized by valence-bond correlations. In the absence of Hund's exchange the model describes a competition between various possible valence-bond states. By considering the clusters with open boundary conditions we demonstrate that orbital interactions are always frustrated, but this frustration is removed by pronounced spin singlet correlations which coexist with supporting them dimer orbital correlations. Such local configurations contribute to the disordered ground states found for the clusters with periodic boundary conditions which interpolate between a highly resonating, dimer-based, entangled spin-orbital liquid phase, and a valence-bond state with completely static spin-singlet states. We argue that these states are also realized for the infinite lattice and anticipate that pronounced transitions between different regimes found for particular geometries will turn out to smooth crossovers in the properties of the spin-orbital liquid in the thermodynamic limit. Finally, we provide evidence that the resonating spin-orbital liquid phase involves entangled states on the bonds. In such a phase classical considerations based on the mean-field theory cannot be used, spin exchange interactions do not determine spin bond correlations, and quantum fluctuations play a crucial role in the ground states and magnetic transitions.

*Published in: Physical Review B* **83**, 094406 (2011).

PACS numbers: 75.10.Kt, 03.65.Ud, 64.70.Tg, 75.10.Jm

## I. SPIN-ORBITAL FRUSTRATION

Frustration in magnetic systems is usually of geometrical origin, but it may also arise due to competing exchange interactions.<sup>1-5</sup> A common feature of frustrated spin systems is that the interactions along different bonds compete with one another, and this leads in some cases to disordered states and to quantum phase transitions when the interaction strength is varied. Another possibility is so-called "order-by-disorder", and several microscopic mechanisms which stabilize ordered state in spin systems have been investigated.<sup>2-5</sup> Here we shall focus on the triangular lattice, where frustrated interactions suggest that valence-bond configurations in spin model with antiferromagnetic (AF) interactions could play an important role,<sup>6</sup> and we supplement them in this work by the frustrated orbital degrees of freedom.

Recently interesting physical realizations of frustrated interactions were introduced in the context of spin-orbital superexchange which arises in transition metal oxides with active orbital degrees of freedom.<sup>7,8</sup> In such models frustration is intrinsic and follows from the directional nature of orbital interactions.<sup>9</sup> Therefore, the orbital part of the spin-orbital superexchange is frustrated even *without* any geometrical frustration. Generic features of this

direction-dependent interactions are captured within the two-dimensional (2D) quantum compass model,<sup>10</sup> which exhibits a quantum phase transition through an isotropic point with highly degenerate ground state (GS).<sup>11-13</sup> This high degeneracy is a fingerprint of highly frustrated interactions and occurs also in the one-dimensional (1D) compass model.<sup>14</sup> It is also characterized by a rather surprising hidden dimer order in the GS which follows from the symmetry of compass interactions.<sup>15</sup>

Frustration in the orbital superexchange models is somewhat more subtle — the interactions depend on the type of active orbital degree of freedom and in each case differ from those in the quantum compass model. In case of  $e_g$  orbitals the interactions are directional as in the quantum compass model, but they are Ising-type only for one cubic axis, e.g. for the bonds  $\langle ij \rangle$  along the  $c$  cubic axis one has the interaction  $\propto \sigma_i^z \sigma_j^z$ , while for the bonds  $\langle ij \rangle$  in the  $ab$  planes they involve linear combinations of  $\{\sigma_i^z, \sigma_i^x\}$  operators which arise from the directional orbital states along the considered ( $a$  or  $b$ ) axis<sup>9,16</sup> (here  $\sigma_i^z$  and  $\sigma_i^x$  are Pauli matrices). This particular structure follows from the fact that although only one of  $e_g$  orbital states participates in charge excitations along each single cubic axis and the interactions appear to be classical in a 1D  $e_g$  orbital model,<sup>17</sup> their superposition is quan-

tum either in a 2D model,<sup>18</sup> or in a three-dimensional one.<sup>19</sup> In contrast, two  $t_{2g}$  orbitals are active and participate in charge excitations along each cubic direction, so the respective interactions involve *a priori* all three components of the orbital pseudospin  $\tau = 1/2$  doublet, with the restriction that the active orbital  $t_{2g}$  doublet changes with the cubic axis.<sup>20</sup> For instance, where the degeneracy of  $t_{2g}$  orbitals is removed by crystal field in the vanadium perovskites and  $xy$  orbitals are filled, the  $\{yz, zx\}$  orbital doublet contributes with orbital fluctuations to the bonds along the  $c$  axis.<sup>21,22</sup>

Realistic superexchange models for perovskite transition metal oxides include both orbital and spin degrees of freedom, which are strongly interrelated.<sup>7,23</sup> Two important questions for these models are: (i) whether the orbital frustration can be removed by properly selected spin states, or frustration is even enhanced by spin-orbital quantum fluctuations, and (ii) to what extent spin dynamics may be treated as independent of orbital dynamics.<sup>24</sup> The disordered GS was suggested for the  $t_{2g}$  orbitals in  $d^1$  configuration on the perovskite lattice.<sup>20</sup>

In the present paper we want to focus on the model derived for the transition metal ions in  $d^1$  configuration for the triangular lattice,<sup>25</sup> with frustration being both of orbital and geometrical origin. This spin-orbital model corresponds to the undistorted  $\text{NaTiO}_2$  and describes magnetic interactions in the spin-orbital space, with superexchange and direct exchange. In the direct exchange case the model is exactly solvable and the GS was determined by considering the dimer coverings of the lattice, with each dimer containing a spin singlet accompanied by two active orbitals on the direct exchange bond.<sup>26</sup> In a general case the GS and the ratio of superexchange and direct exchange are not known — the latter depends on the respective effective hopping elements via the oxygen orbitals responsible for the superexchange and the ( $dd\sigma$ ) hopping which gives the direct exchange. Therefore, we use it below as a model parameter. A second parameter of the spin-orbital model considered here is Hund's exchange interaction. One might expect that also in case of superexchange interactions  $t_{2g}$  orbitals could order and remove the frustration in the triangular lattice, as they do, for instance, in  $\text{LiVO}_2$ .<sup>27</sup> It was argued, however, in Ref. 25 that the GS of the present  $d^1$  spin-orbital model is disordered and dominated by dimer correlations practically for any ratio of the superexchange and direct exchange interaction. This conclusion was drawn by considering the mean-field (MF) states, variational wave functions with valence-bond correlations, and exact diagonalization of small systems of not more than  $N = 4$  sites.

The purpose of this paper is to reanalyze the spin-orbital states in the  $d^1$  spin-orbital model on the triangular lattice,<sup>25</sup> and provide evidence in favor of the disordered spin-orbital liquid GS from numerical studies of larger finite systems, having up to  $N = 10$  sites. We use extensively Lanczos diagonalization, but for rather small systems of size up to  $N = 6$  sites where full diagonaliza-

tion is also possible in the subspace of  $\mathcal{S}^z = 0$  total spin, both methods were compared with each other. Thereby, we addressed a few general questions which concern the spin-orbital physics for varying parameters of the model: (i) nature of dimer spin and orbital correlations, (ii) nature of the transition to the spin-polarized ferromagnetic (FM) state with increasing Hund's exchange, (iii) importance of spin-orbital entanglement<sup>24</sup> and its consequences for the transition from low-spin to high-spin states. We will provide answers to these questions by considering systems of various size and with different boundary conditions. Altogether, we shall demonstrate that quantum fluctuations determine the GS and the magnetic transitions to such an extent that classical considerations cannot be used in several situations.

The paper is organized as follows. In Sec. II A we introduce the  $d^1$  spin-orbital model on a triangular lattice (as for  $\text{Ti}^{3+}$  or  $\text{V}^{4+}$  ions) as derived in Ref. 25. Basic information about the cluster sizes and geometries used in Lanczos diagonalization is contained in Sec. II B. The numerical results obtained for the isolated clusters of up to  $N = 10$  sites are analyzed in Sec. III. In this section we investigate the model in absence of Hund's exchange and analyze bond correlations: spin, orbital and spin-orbital ones, as well as the orbital occupation. They allowed us to find certain general trends which are expected to determine the behavior of the model in the thermodynamic limit. The generic transition from quantum to classical regime in the singlet sector, with interactions evolving from superexchange to direct exchange, is illustrated by a hexagonal cluster in Sec. III A. Next we consider triangular clusters with open boundary conditions in Sec. III B and show that the singlet correlations are robust in the entire regime of the exchange interactions. The results obtained for the clusters with periodic boundary conditions are reported in Sec. III C. In Sec. IV A we present the orbital model obtained in spin polarized case, and investigate the transition from low-spin to high-spin states for a few representative clusters, presenting the respective phase diagrams in Sec. IV B. Finally, we present the consequences of spin-orbital entanglement in Sec. V A and show that it modifies the phase diagrams significantly with respect to those obtained when spin and orbital operators are disentangled, particularly in the regime of purely superexchange interactions. We also point out in Sec. V B that meaningful exchange constants cannot be introduced in cases where spin-orbital entanglement dominates and stabilizes the low-spin ground state with large spin-orbital fluctuations. General discussion and summary are presented in Sec. VI.

## II. SPIN-ORBITAL MODEL

### A. Superexchange versus direct exchange

We consider the spin-orbital model on the triangular lattice derived in Ref. 25 which describes interactions between  $S = 1/2$  spins for  $d^1$  electron configurations, such as in NaTiO<sub>2</sub>. The magnetic transition metal ions form a triangular lattice for the  $\langle 111 \rangle$  planes of a compound with cubic symmetry. The bonds  $\langle ij \rangle$  are spanning the three directions, labeled by  $\gamma = a, b, c$ .

In order to explain the physical content of the model we consider a representative bond along the  $c$  axis shown in Fig. 1(a). For the realistic parameters of NaTiO<sub>2</sub> the  $3d$  electrons are almost localized in  $d^1$  configurations of Ti<sup>3+</sup> ions, hence their interactions with neighboring sites can be described by the effective superexchange and kinetic exchange processes. Virtual charge excitations,  $d_i^1 d_j^1 \rightleftharpoons d_i^2 d_j^0$ , between the neighboring sites generate magnetic interactions which arise from two different hopping processes for active  $t_{2g}$  orbitals: (i) the effective hopping  $t = t_{pd}^2/\Delta$  which occurs via oxygen  $2p_z$  orbitals with the charge transfer excitation energy  $\Delta$  and consists of two  $t_{pd}$  steps,<sup>28</sup> in the present case along the 90° bonds, and (ii) direct hopping  $t'$  which couples the  $t_{2g}$  orbitals along the bond and give direct (kinetic exchange) interaction. Note that the latter processes couple orbitals with the same flavor, while the former ones couple different orbitals, and there the occupied orbitals may be interchanged as a result of a virtual charge excitation.

For convenience, we introduce the notation

$$|a\rangle \equiv |yz\rangle, \quad |b\rangle \equiv |xz\rangle, \quad |c\rangle \equiv |xy\rangle, \quad (2.1)$$

for the three  $t_{2g}$  orbital flavors (colors), following the one used in the perovskite systems,<sup>20</sup> adopted here for the triangular lattice.<sup>29</sup> It follows from the symmetry of orbital wave functions that only two of the three  $t_{2g}$  orbitals allow for  $d-p$  hopping  $t_{pd}$  and are active in superexchange on any given bond  $\langle ij \rangle$  [Fig. 1(b)], while the remaining  $\gamma$  orbitals couple directly along the  $\gamma$  axis, so they contribute to the direct (kinetic) exchange, see Fig. 1(c). In addition, each site is occupied by precisely one electron, so the density operators satisfy a local constraint at each site  $i$ ,

$$n_{ia} + n_{ib} + n_{ic} \equiv 1. \quad (2.2)$$

These symmetry properties on the triangular lattice are analogous to those which decide about the form of the kinetic energy for  $t_{2g}$  electrons in the perovskite lattice.<sup>20,21</sup>

Local Coulomb interactions at transition metal ions are described by two parameters: intraorbital Coulomb interaction  $U$  and Hund's exchange  $J_H$ .<sup>30</sup> In the limit of large intraorbital Coulomb interaction  $U$  intersite charge excitations are transformed away and one finds the following Hamiltonian,<sup>25</sup>

$$\mathcal{H} = J \left\{ (1 - \alpha) \mathcal{H}_s + \sqrt{(1 - \alpha)\alpha} \mathcal{H}_m + \alpha \mathcal{H}_d \right\}, \quad (2.3)$$

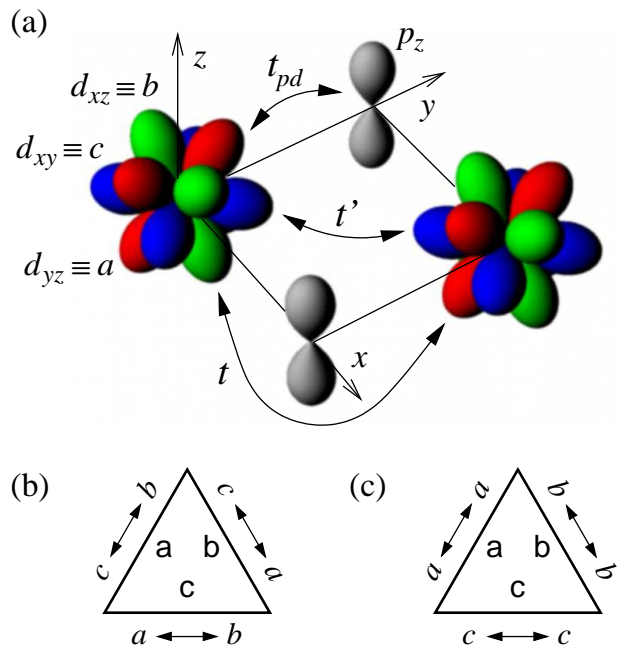


FIG. 1: (Color online) (a) Schematic view of the hopping processes between  $t_{2g}$  orbitals along a bond parallel to the  $c$  axis in NaTiO<sub>2</sub>: (i)  $t_{pd}$  between Ti( $t_{2g}$ ) orbitals and O( $2p_z$ ) orbitals, with two  $t_{pd}$  transitions contributing to an effective hopping  $t$ , and (ii) direct  $d-d$  hopping  $t'$ . The hopping  $t$  interchanges two orbital flavors on two sites and contributes to the effective superexchange interactions on a bond in the triangular lattice, while the latter (diagonal) hopping element  $t'$  contributes to the direct (kinetic) exchange. The  $t_{2g}$  orbitals are shown by different gray scale (color) and are labeled as  $a$ ,  $b$ , and  $c$ , see Eq. (2.1). In the bottom part the hopping processes contributing to (b) superexchange and (c) direct exchange, are shown for the bonds along  $\gamma = a, b, c$  axes in the triangular lattice.

where  $J$  is the exchange energy. The parameter  $\alpha$  is the first parameter of the present model Eq. (2.3) and is given by the hopping elements as follows,

$$\alpha = \frac{t'^2}{t^2 + t'^2} \quad (2.4)$$

— it interpolates between the superexchange ( $\alpha = 0$ ) and direct exchange ( $\alpha = 1$ ) limit, as explained in Ref. 25. The second parameter of the spin-orbital model Eq. (2.3) is Hund's exchange,

$$\eta = \frac{J_H}{U}. \quad (2.5)$$

It enters the superexchange and direct exchange (see below) via the coefficients

$$r_1 = \frac{1}{1 - 3\eta}, \quad r_2 = \frac{1}{1 - \eta}, \quad r_3 = \frac{1}{1 + 2\eta}, \quad (2.6)$$

which follow from the multiplet structure of  $d^2$  ions.<sup>31</sup> They correspond to the triplet excitation at energy ( $U -$

$3J_H$ ), and to singlet excitations at energies  $(U - J_H)$  and  $(U + 2J_H)$ . Although the actual values of the Coulomb and Hund's exchange elements were deduced from the spectroscopic data for  $\text{Ti}^{2+}$  ions corresponding to charge excitations by Zaanen and Sawatzky,<sup>32</sup>  $U = 4.35$  eV and  $J_H = 0.59$  eV, which gives a value of  $\eta \simeq 0.14$ , we shall use  $\eta$  as a parameter below in order to investigate the transition from low-spin to high-spin states for various cluster size and to highlight the difference in the orbital correlations in the low and high  $\eta$  regime.

The superexchange part of  $\mathcal{H}$  can be specified as follows

$$\begin{aligned} \mathcal{H}_s = & \frac{1}{2} \sum_{\langle ij \rangle \parallel \gamma} \left\{ r_1 \left( \vec{S}_i \cdot \vec{S}_j + \frac{3}{4} \right) \left[ A_{ij}^{(\gamma)} + \frac{1}{2} (n_{i\gamma} + n_{j\gamma}) - 1 \right] \right. \\ & + r_2 \left( \vec{S}_i \cdot \vec{S}_j - \frac{1}{4} \right) \left[ A_{ij}^{(\gamma)} - \frac{1}{2} (n_{i\gamma} + n_{j\gamma}) + 1 \right] \\ & \left. - \frac{2}{3} (r_2 - r_3) \left( \vec{S}_i \cdot \vec{S}_j - \frac{1}{4} \right) B_{ij}^{(\gamma)} \right\}, \end{aligned} \quad (2.7)$$

and contains two spin operators — a projection on the triplet state  $(\vec{S}_i \cdot \vec{S}_j + \frac{3}{4})$ , and an operator  $-(\vec{S}_i \cdot \vec{S}_j - \frac{1}{4})$  which is a projection on the singlet state. These operators accompany the coefficients  $\{r_1, r_2, r_3\}$  and express the dependence on the excited  $d^2$  states.

The orbital operators  $A_{ij}$  and  $B_{ij}$  in Eq. (2.7) depend on the bond direction  $\gamma$  and involve two orbital flavors active in the superexchange,

$$A_{ij}^{(\gamma)} = \left( T_{i\gamma}^+ T_{j\gamma}^+ + T_{i\gamma}^- T_{j\gamma}^- \right) - 2T_{i\gamma}^z T_{j\gamma}^z + \frac{1}{2} n_i^{(\gamma)} n_j^{(\gamma)}, \quad (2.8)$$

$$B_{ij}^{(\gamma)} = \left( T_{i\gamma}^+ T_{j\gamma}^- + T_{i\gamma}^- T_{j\gamma}^+ \right) - 2T_{i\gamma}^z T_{j\gamma}^z + \frac{1}{2} n_i^{(\gamma)} n_j^{(\gamma)}. \quad (2.9)$$

The operator  $n_{i\gamma}$  in Eq. (2.7) stands for the number of electrons at site  $i$  in the orbital *inactive* in superexchange processes, for instance  $n_{i\gamma} \equiv n_{ic}$  in the example depicted in Fig. 1. On the contrary,  $n_i^{(\gamma)}$  is the total electron number operator at site  $i$  for orbitals *active* in superexchange, i.e., in the case shown in Fig. 1 it is  $n_i^{(c)} = n_{ia} + n_{ib}$ . The orbital operators  $\{T_{i\gamma}^+, T_{i\gamma}^-, T_{i\gamma}^z\}$  refer to the orbital doublet active in the superexchange on the bond  $\langle ij \rangle \parallel \gamma$ . For a single bond, the orbital operators in Eqs. (2.8) and (2.9) may be written in a very suggestive form by performing a local transformation in which the active orbitals are exchanged on one bond site,<sup>29</sup> e.g.  $|a\rangle \rightarrow |b\rangle$  and  $|b\rangle \rightarrow |a\rangle$  on bond  $\langle ij \rangle \parallel c$ :

$$A_{ij}^{(\gamma)} \equiv 2 \left\{ \left( \vec{T}_i \cdot \vec{T}_j \right)^{(\gamma)} + \frac{1}{4} n_i^{(\gamma)} n_j^{(\gamma)} \right\}, \quad (2.10)$$

$$B_{ij}^{(\gamma)} \equiv 2 \left\{ \left( \vec{T}_i \odot \vec{T}_j \right)^{(\gamma)} + \frac{1}{4} n_i^{(\gamma)} n_j^{(\gamma)} \right\}. \quad (2.11)$$

Here the scalar product in  $A_{ij}$  is the conventional expression for pseudospin  $T = 1/2$  variables transformed as described above, and the product in  $B_{ij}$  is the usual term which follows from the structure of local Coulomb

interactions, as well transformed — they are defined as follows:

$$\left( \vec{T}_i \cdot \vec{T}_j \right)^{(\gamma)} \equiv \frac{1}{2} \left( T_{i\gamma}^+ T_{j\gamma}^- + T_{i\gamma}^- T_{j\gamma}^+ \right) + T_{i\gamma}^z T_{j\gamma}^z, \quad (2.12)$$

$$\left( \vec{T}_i \odot \vec{T}_j \right)^{(\gamma)} \equiv \frac{1}{2} \left( T_{i\gamma}^+ T_{j\gamma}^+ + T_{i\gamma}^- T_{j\gamma}^- \right) + T_{i\gamma}^z T_{j\gamma}^z, \quad (2.13)$$

This form follows from the local transformation at site  $j$  which is introduced for the superexchange in the present case.<sup>29</sup> These operators select favored orbital configurations on two neighboring sites via the  $T_{i\gamma}^z T_{j\gamma}^z$  terms, and orbital fluctuations are described by the  $T_{i\gamma}^\pm T_{j\gamma}^\mp$  and  $T_{i\gamma}^\pm T_{j\gamma}^\pm$  terms. Note that the  $z$ -th pseudospin component is not conserved. For a bond along the axis  $\gamma$  orbital operators at site  $i$  are defined by the electron creation  $\{a_i^\dagger, b_i^\dagger, c_i^\dagger\}$  and annihilation  $\{a_i, b_i, c_i\}$  operators for fermions with a given flavor. For instance, for the bonds along the  $a$  or  $b$  axis they are:

$$\begin{aligned} T_{ia}^+ &= b_i^\dagger c_i, & T_{ib}^+ &= c_i^\dagger a_i, \\ T_{ia}^- &= c_i^\dagger b_i, & T_{ib}^- &= a_i^\dagger c_i, \end{aligned} \quad (2.14)$$

$$T_{ia}^z = \frac{1}{2} (n_{ib} - n_{ic}), \quad T_{ib}^z = \frac{1}{2} (n_{ic} - n_{ia}). \quad (2.15)$$

The direct (kinetic) exchange term involves only virtual excitations of  $\gamma$  orbitals on a bond  $\langle ij \rangle \parallel \gamma$ ,

$$\begin{aligned} \mathcal{H}_d = & \frac{1}{4} \sum_{\langle ij \rangle \parallel \gamma} \left\{ \left[ -r_1 \left( \vec{S}_i \cdot \vec{S}_j + \frac{3}{4} \right) + r_2 \left( \vec{S}_i \cdot \vec{S}_j - \frac{1}{4} \right) \right] \right. \\ & \times \left[ n_{i\gamma} (1 - n_{j\gamma}) + (1 - n_{i\gamma}) n_{j\gamma} \right] \\ & \left. + \frac{1}{3} (2r_2 + r_3) \left( \vec{S}_i \cdot \vec{S}_j - \frac{1}{4} \right) 4n_{i\gamma} n_{j\gamma} \right\}. \end{aligned} \quad (2.16)$$

Therefore the structure of the orbital operators is here simpler — they enter as projection operators and give two different individual terms:<sup>25</sup> either (i) when only one active orbital is occupied,  $\propto n_{i\gamma} (1 - n_{j\gamma})$ , or (ii) when both orbitals are occupied,  $\propto n_{i\gamma} n_{j\gamma}$ . For the bond shown in Fig. 1  $\gamma \equiv c$ . The structure of  $d^2$  excited states is here the same as for the superexchange, so the same coefficients given in Eqs. (2.6) occur in both terms, superexchange Eq. (2.7) and kinetic exchange Eq. (2.16).

As explained in Ref. 25, the two different types of hopping processes ( $t$  and  $t'$ ) may contribute in a two-step virtual  $d_i^1 d_j^1 \rightleftharpoons d_i^2 d_j^0$  excitation, in such a way that the occupied orbitals are changed at both sites. In such a case the resulting effective interaction are expressed in terms of orbital fluctuation operators. For the bond shown in Fig. 1 these terms are:

$$\begin{aligned} \mathcal{H}_m^{(c)} = & -\frac{1}{4} \sum_{\langle ij \rangle \parallel c} \left\{ r_1 \left( \vec{S}_i \cdot \vec{S}_j + \frac{3}{4} \right) - r_2 \left( \vec{S}_i \cdot \vec{S}_j - \frac{1}{4} \right) \right\} \\ & \times \left( T_{ia}^+ T_{jb}^+ + T_{ib}^- T_{ja}^- + T_{ib}^+ T_{ja}^+ + T_{ia}^- T_{jb}^- \right), \end{aligned} \quad (2.17)$$

where the orbital operators are defined in Eqs. (2.14). The form of the  $\mathcal{H}_m^{(a)}$  and  $\mathcal{H}_m^{(b)}$  terms is obtained from Eq.

(2.17) by cyclic permutations of the orbital indices. Note that these terms describe fluctuations that go *beyond* any static orbital configuration, so they represent corrections to the classical treatment of the spin-orbital correlations, as discussed in Secs. V A and V B.

In the subsequent sections we will focus first on the frustrated interactions in the model of Eq. (2.3) at  $\eta = 0$ . This case is rather special as the multiplet structure collapses to a single excitation with energy  $U$  (spin singlet and triplet excitations are then degenerate), and the Hamiltonian depends only on the ratio of superexchange to direct exchange, parametrized by  $0 \leq \alpha \leq 1$ , and has the following form:

$$\begin{aligned} \mathcal{H}_0 = J \sum_{\langle ij \rangle \parallel \gamma} & \left\{ (1 - \alpha) \left[ 2 \left( \vec{S}_i \cdot \vec{S}_j + \frac{1}{4} \right) \right. \right. \\ & \times \left[ \left( \vec{T}_i \cdot \vec{T}_j \right)^{(\gamma)} + \frac{1}{4} n_i^{(\gamma)} n_j^{(\gamma)} \right] + \frac{1}{2} (n_{i\gamma} + n_{j\gamma}) - 1 \left. \right] \\ & + \alpha \left[ \left( \vec{S}_i \cdot \vec{S}_j - \frac{1}{4} \right) n_{i\gamma} n_{j\gamma} \right. \\ & \left. - \frac{1}{4} (n_{i\gamma} (1 - n_{j\gamma}) + (1 - n_{i\gamma}) n_{j\gamma}) \right] \\ & \left. - \frac{1}{4} \sqrt{\alpha(1 - \alpha)} \left( T_{i\bar{\gamma}}^+ T_{j\bar{\gamma}}^+ + T_{i\bar{\gamma}}^- T_{j\bar{\gamma}}^- + T_{i\bar{\gamma}}^+ T_{j\bar{\gamma}}^- + T_{i\bar{\gamma}}^- T_{j\bar{\gamma}}^+ \right) \right\}. \end{aligned} \quad (2.18)$$

Here the orbital scalar product  $\left( \vec{T}_i \cdot \vec{T}_j \right)^{(\gamma)}$  is given by Eq. (2.12). The Hamiltonian  $\mathcal{H}_0$  describes AF interactions between spins, but the orbital terms favor either orbital fluctuations (superexchange) or a static configuration of the same orbitals (direct exchange) on the bond. The form of the superexchange  $\propto (1 - \alpha)$  suggests that the spin and orbital sectors could be completely equivalent and symmetrical at  $\alpha = 0$  for a single bond. However, this remains true only as long as active orbitals can be selected to contribute to the superexchange as this bond, i.e., for  $n_i^{(\gamma)} n_j^{(\gamma)} \equiv 1$ , and this equivalence is broken when more bonds are considered.<sup>25</sup>

A remarkable feature of the Hamiltonian Eq. (2.18) is the lack of higher symmetry in any of the points when  $\alpha$  is varied. Even at  $\alpha = 0.5$ , where all electron transitions have the same amplitude, no higher symmetry occurs as the superexchange ( $\alpha = 0$ ) and direct exchange  $\alpha$  result from quite distinct processes and cannot be transformed into each other. The only analytical solution was found in  $\alpha = 1$  case, where at  $\eta = 0$  the extremely degenerate GS is a liquid of hard-core dimers.<sup>26</sup> This degeneracy is removed at  $\eta > 0$ , and a valence-bond crystal with a large unit cell of 20 sites is formed.

## B. Lanczos diagonalization and cluster size

In order to establish unbiased results concerning the nature of the GS and spin and orbital correlations in the

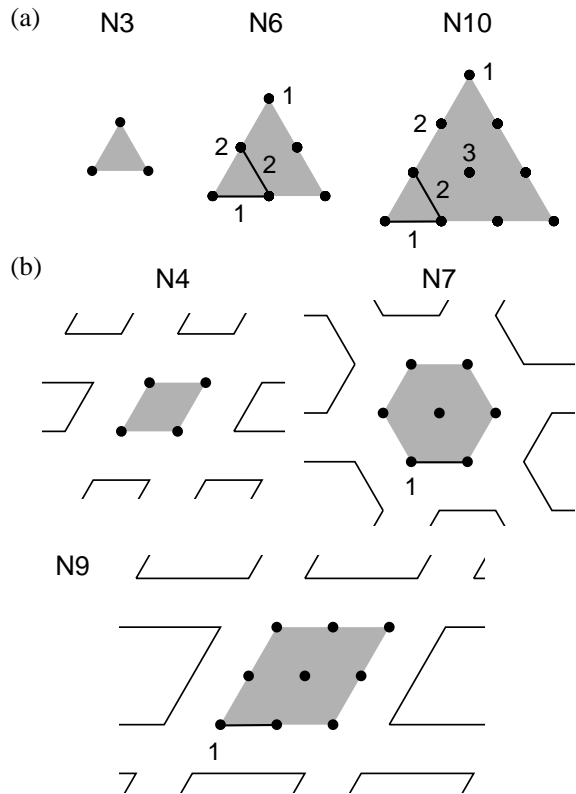


FIG. 2: Clusters (shown in gray) used to investigate the spin-orbital model (2.3) by full or Lanczos exact diagonalization: (a) triangular clusters with open boundary conditions N3, N6 and N10 — here nonequivalent sites and bonds used later are indicated by labels 1, 2 and 3, and (b) clusters with periodic boundary conditions: rhombic N4, hexagonal N7 and rhombic N9. In the latter case positions of neighboring clusters which cover the triangular lattice are indicated and all the sites and bonds are equivalent (label 1 is used for equivalent sites and bonds in N7 and N9 clusters).

present spin-orbital model Eq. (2.3), providing evidence in favor of spin-orbital liquid state, we have used diagonalization of finite clusters. As the number of degrees of freedom per site is  $2 \times 3 = 6$ , the size of the Hilbert space increases very fast with increasing system size  $N$ . The only symmetry which could straightforwardly be implemented is the conservation of the  $z$ -th component of total spin,

$$\mathcal{S}^z = \sum_{i=1}^N S_i^z, \quad (2.19)$$

while the orbital state is *a priori* undetermined. Therefore, the use of full exact diagonalization is practically limited to system of up to  $N = 6$  sites, where the size of the Hilbert space is  $6^6 = 46656$  and the largest ( $\mathcal{S}^z = 0$ ) subspace has the dimension 14580. The use of the Lanczos method allowed us to investigate systems of up to  $N = 10$  sites.

Although several other clusters were studied as well, we would like to concentrate here only on two classes

of clusters which help to identify certain general trends for the present spin-orbital model. First of them are triangular clusters with open boundary conditions (OBC) which by construction have nonequivalent sites and are expected to favor dimer correlations. They were used to identify the dimer correlations and to find their evolution with increasing size. These clusters help to understand the interrelation between spin and orbital states on the bonds which become transparent when the symmetry in the orbital space is broken by geometry. The clusters considered here contain  $N = 3, 6, 10$  sites and are labeled N3, N6 and N10, see Fig. 2(a).

The second class of clusters, shown in Fig. 2(b), consists of three clusters with up to 9 sites which cover entirely the triangular lattice and can thus be investigated using periodic boundary conditions (PBC): rhombic cluster N4, hexagonal cluster N7, and large rhombic cluster N9. However, the PBC are not unique and, as we have verified, lead to nonequivalent results. Therefore we selected in each case displayed in Fig. 2(b) such PBC which result from ordering the considered clusters in rows on the triangular lattice, as indicated by the clusters surrounding the one used for Lanczos (or full) diagonalization. Unlike some other lattice coverings, these boundary conditions guarantee that all the bonds and sites are equivalent in each considered cluster. Therefore, no additional frustration of interactions is introduced by selecting the PBC and the internal symmetry of the considered cluster is preserved. Hence, we suggest that these clusters may serve to simulate the situation in the thermodynamic limit.

### C. Correlation functions and entanglement

In Secs. III-IV we will compute and discuss the GSs of several clusters, by looking at their energies, degeneracies, site occupations, as well as the spin, orbital and spin-orbital (four-operator) correlation functions for a bond  $\langle ij \rangle$  along  $\gamma$  axis, given respectively by

$$S_{ij} \equiv \frac{1}{d} \sum_n \langle n | \vec{S}_i \cdot \vec{S}_j | n \rangle, \quad (2.20)$$

$$T_{ij} \equiv \frac{1}{d} \sum_n \langle n | (\vec{T}_i \cdot \vec{T}_j)^{(\gamma)} | n \rangle, \quad (2.21)$$

$$\begin{aligned} C_{ij} &\equiv \frac{1}{d} \sum_n \langle n | (\vec{S}_i \cdot \vec{S}_j - S_{ij})(\vec{T}_i \cdot \vec{T}_j - T_{ij})^{(\gamma)} | n \rangle \\ &= \frac{1}{d} \sum_n \langle n | (\vec{S}_i \cdot \vec{S}_j)(\vec{T}_i \cdot \vec{T}_j)^{(\gamma)} | n \rangle \\ &\quad - \frac{1}{d} \sum_n \langle n | \vec{S}_i \cdot \vec{S}_j | n \rangle \frac{1}{d} \sum_m \langle m | (\vec{T}_i \cdot \vec{T}_j)^{(\gamma)} | m \rangle, \end{aligned} \quad (2.22)$$

where  $d$  is the GS degeneracy, and the pseudospin scalar product in Eqs. (2.21) and (2.22) is defined by Eq. (2.12). In clusters with OBC the correlations depend on the bond, but for the clusters with PBC all the bonds are

equivalent and these correlations are uniform. The summations include all independent quantum states  $\{|n\rangle\}$  which span the possibly degenerate GS manifold.

The degeneracy  $d$  of the GS and the corresponding state vectors are easily obtained if full exact diagonalization can be used. On the other hand, due to appearance of spurious degeneracies, the Lanczos diagonalization in its basic form is not able to quantify reliably the degeneracy and to generate the set of suitable GS vectors. In the present work we have used the following way to remedy this problem: The Lanczos algorithm is performed several times using random initial vectors and a sufficient number of the GS vectors is generated. The orthonormalization of this set then yields the degeneracy of the GS as the number of independent vectors and the orthonormal GS vectors themselves can be used in the GS averaging implied by Eqs. (2.20)-(2.22). Furthermore, it is possible to determine the range of possible values of the quantities of interest within the GS manifold. This is achieved by evaluating the minimum and maximum eigenvalue of the matrix representing the corresponding operator within this manifold. In such cases the obtained ranges of possible values are indicated in all the relevant figures in a form of vertical lines.

The last correlation function  $C_{ij}$  Eq. (2.22) quantifies the average difference between the complete spin-orbital operator and its decoupled product. Therefore, we use it here as the simplest measure of spin-orbital entanglement. If  $C_{ij} = 0$ , the MF decoupling of spin and orbital operators on the bond  $\langle ij \rangle$  is exact and both subsystems may be treated independently from each other. This implies that the GS wave function can be written as a product of its spin and orbital parts. For instance, this happens for the high-spin states which become the GS at large  $\eta$ .<sup>24</sup>

However, we note that the criterion of spin-orbital entanglement introduced above as  $C_{ij} \neq 0$  can be rigorously applied only for systems with nondegenerate GS ( $d = 1$ ). If  $d > 1$ , the averaging introduced in  $S_{ij}$  and  $T_{ij}$ , used in Eq. (2.22), means that  $C_{ij}$  could be (small but) finite even in cases when spin-orbital *de facto* decoupling takes place, and the measure of entanglement would have to be more subtle. Nevertheless, we use here  $C_{ij}$  Eq. (2.22) as a simple diagnostic tool, and comment in more detail on particular cases, where  $C_{ij} \neq 0$ .

## III. TOWARD SPIN-ORBITAL LIQUID

### A. Quantum and classical dimers in a hexagonal cluster

In order to understand the consequences of frustration on spin, orbital and spin-orbital correlations on the triangular lattice it is instructive to start with analyzing a simpler case of a honeycomb lattice, where the geometrical frustration is absent.<sup>25</sup> A representative cluster for such a lattice is a hexagonal cluster H6 (obtained from

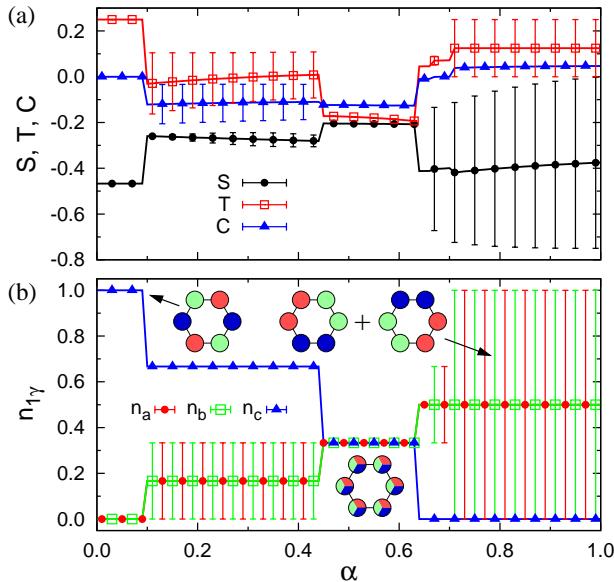


FIG. 3: (Color online) Evolution of the GS for a hexagon H6 with OBC as a function of  $\alpha$  in the absence of Hund's exchange ( $\eta = 0$ ): (a) bond correlations — spin  $S_{ij}$  Eq. (2.20), circles, orbital  $T_{ij}$  Eq. (2.21), squares, and spin-orbital  $C_{ij}$  Eq. (2.22), triangles; (b) orbital electron densities  $n_{1\gamma}$  at site  $i = 1$  (left-most site):  $n_{1a}$  (circles),  $n_{1b}$  (squares),  $n_{1c}$  (triangles). The insets indicate the orbital configurations realized in the superexchange limit ( $\alpha = 0$ ), for  $0.44 < \alpha < 0.63$ , and in the direct exchange limit ( $\alpha = 1$ ). The vertical lines indicate the range of possible values of the particular quantity (bond correlation or electron density). They should not be confused with any kind of numerical error as they indicate an exactly determined range due to the GS degeneracy.

the N7 cluster in Fig. 2(b) by removing the central site) which will be considered here with OBC. It serves to unravel the generic behavior of the orbital correlations for increasing  $\alpha$  and to investigate the spin-orbital entanglement in different parameter regimes of the spin-orbital model Eq. (2.3). This cluster was analyzed using Lanczos diagonalization, and we present also the degeneracy of the GS below.

One finds that all the orbitals contribute equally in the entire range of  $\alpha$ , and each orbital state is occupied at two out of six sites in the GS, in the entire regime of  $\alpha$ . However, the orbital state changes under increasing  $\alpha$  and one finds four distinct regimes by analyzing the evolution of the GS shown by the correlation functions and orbital densities displayed in Fig. 3. The transitions between them are abrupt (first order) and occur by level crossing. Each site in the hexagonal cluster participates only in two bonds which breaks the spatial symmetry in the orbital space in a particular way. In the superexchange model at  $\alpha = 0$  there is precisely one orbital at each site which contributes to the interactions along both bonds, and we have found that indeed  $n_{i\gamma} = 1$  for this particular orbital [for site  $i = 1$ ,  $c$  orbital is active along both bonds, as shown in Fig. 1(b)]. This results in a unique

GS which is characterized by a frozen orbital configuration and triplet orbital correlations at each bond  $\langle ij \rangle$ , i.e.,  $T_{ij}^\gamma = 0.25$ , see Fig. 3(a). Under these circumstances the orbitals decouple from spins and Eq. (2.18) reduces to the AF Heisenberg model on this cluster. Therefore, the GS is disentangled, with  $C_{ij} = 0$ , and one finds that the spin correlations are exactly the same as for the 1D chain of  $N = 6$  sites with PBC, i.e.,  $S_{ij} = -0.4671$ .

Orbital fluctuations gradually increase with increasing  $\alpha$ , but the above GS remains stable up to  $\alpha \simeq 0.10$ . For larger  $0.10 < \alpha < 0.44$  the fluctuations "soften" the orbital state and allow for local fluctuations along the bonds. As spins are also involved, this change of the GS is not gradual but occurs as a quantum transition to the state with degeneracy  $d = 2$ . In this GS the spin correlations weaken to  $S_{ij} \simeq -0.27$  and the joint spin-and-orbital fluctuations contribute with finite mixed correlation function,  $C_{ij} \simeq -0.12$ , see Fig. 3(a).

The degeneracy of the GS results in different values of the possible orbital occupancy at each site — while the probability of occupying the orbital  $c$  at site 1 is now reduced to  $n_{1c} = 2/3$  in each component, the remaining orbital with finite density is either  $a$  or  $b$ , depending on the actual wave function. Each component satisfies the local constraint given in Eq. (2.2). As a result, the average density  $n_{1a} = n_{1b} = 1/6$  follows from two contributing eigenfunctions, with either  $n_{1a} = 1/3$  or  $n_{1b} = 1/3$ , and the third orbital empty ( $n_{1b} = 0$  or  $n_{1a} = 0$ ). This is marked in Fig. 3(b) by the vertical lines (error bars) which indicate the range of possible values for the relevant electron density  $n_{1\gamma}$ .

In agreement with intuition, when  $\alpha = 0.5$  and all interorbital transitions shown in Fig. 1 have equal amplitude, there is large orbital mixing which is the most prominent feature in the GS found in the intermediate regime of  $0.44 < \alpha < 0.63$ . It is not centered at  $\alpha = 0.5$  as there are less processes which contribute to direct exchange than to superexchange, the energy gain is lower in the direct exchange regime and thus this regime which comes next is narrower. Although both superexchange and direct exchange suggest AF spin couplings, the orbitals fluctuate here strongly and couple to the spins. Therefore, AF spin correlation function is again reduced to  $S_{ij} \simeq -0.21$ . Remarkably, both the orbital correlations,  $T_{ij} \simeq -0.18$ , and the mixed correlations,  $C_{ij} \simeq -0.13$ , are also negative, and the GS is unique ( $d = 1$ ). Here all the orbitals contribute equally and  $n_{1\gamma} = 1/3$ , as seen in the inset of Fig. 3(b). We recognize this state as a prerequisite of the spin-orbital liquid state which dominates the behavior of the triangular lattice, as we demonstrate below in Sec. III C. Actually, there is also some similarity between this fluctuating GS and the GS of the 1D SU(4) spin-orbital model,<sup>24</sup> but here the symmetry is lower by construction.

The regime of larger values of  $\alpha > 0.63$  favors the direct exchange interactions, supported by pairs of identical orbitals active on an exchange bond. Having only one orbital flavor active along each bond, only three bonds

may be occupied by spin singlets and contribute with a direct exchange energy, and there are two distinct configurations with differently distributed orbital occupations along the hexagonal ring, shown in Fig. 3(b). These two distinct GSs (degeneracy  $d = 2$ ) cause again two distributions of the orbital densities, this time varying between 0 and 1 in the majority of the direct exchange regime, i.e., for  $\alpha > 0.7$ . After averaging over two degenerate states, the average occupancy for the orbitals which are active on one of the bonds originating from each site  $i$  is  $n_{ia} = n_{ib} = 0.5$ . However, there is also a narrow range of  $0.63 < \alpha < 0.7$ , where such fluctuations have a lower amplitude, only between  $1/3$  and  $2/3$ . This suggests that the orbital fluctuations play still an important role here and couple weakly since  $C_{ij} \simeq 0.05$ , in contrast to  $\alpha > 0.7$  characterized simply by two distinct orbital configurations and factorized spin and orbital degrees of freedom, i.e.,  $C_{ij} = 0$ . Indeed, as a result of averaging over two degenerate wave functions in the GS, see inset of Fig. 3(b), one finds at  $\alpha = 1$  the bond correlations  $S_{ij} = -3/8$  and  $T_{ij} = 1/8$ . These results demonstrate that two orbital configurations are static.

### B. Triangular clusters with open boundary conditions

In contrast to the hexagonal cluster considered above, triangular clusters of Fig. 2(a) are characterized by frustrated spin-orbital interactions and contain nonequivalent bonds. Therefore the case of decoupled spin and orbital dynamics cannot be realized in the superexchange limit (at  $\alpha = 0$ ) in none of the clusters. In fact, the orbitals try to adjust themselves to the frustrated geometry, but in general several equivalent configurations contribute and the obtained results follow from averaging over them. The smallest triangular cluster N3 was already analyzed in Ref. 25, we therefore concentrate here on N6 and N10. Below we discuss first the bond correlation functions and next explain them by presenting the electron distribution over  $t_{2g}$  orbital states.

The intersite spin, orbital, and spin-orbital correlations are presented in Fig. 4 for two classes of bonds shown in Fig. 2(a): a bond involving a corner site labeled as 1, and an internal bond being close to a corner labeled as 2. In order to simplify the notation we label the respective *bond* correlation functions for a bond  $n = 1, 2$  by a bond index as  $\mathcal{S}_n$ ,  $\mathcal{T}_n$ , and  $\mathcal{C}_n$ , respectively. The data points indicate three physically different regimes (similar to some extent to H6 cluster of Sec. III A): (i) the superexchange regime in a range of small values  $\alpha \geq 0$ , (ii) an intermediate regime for values of  $\alpha$  close to but typically larger than  $\alpha = 0.5$ , and (iii) the direct exchange regime for large values of  $\alpha$  close to  $\alpha = 1$ . The range of values of  $\alpha$  for each of these three regimes depends on the cluster size, but certain common features can easily be recognized in Fig. 4. Altogether, the intermediate regime where the electrons are almost equally distributed

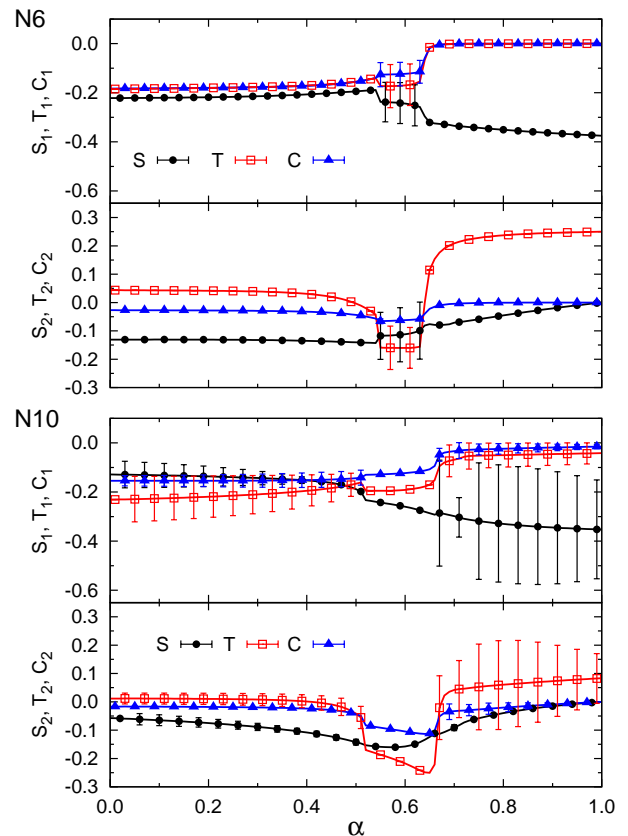


FIG. 4: (Color online) Bond correlations for triangular clusters for increasing  $\alpha$  in absence of Hund's exchange ( $\eta = 0$ ), as obtained for topologically equivalent bonds  $n = 1, 2$  in triangular clusters N6 (top) and N10 (bottom) with OBC, see Fig. 2(a): spin ( $\mathcal{S}_n$ , circles), orbital ( $\mathcal{T}_n$ , squares), and spin-orbital ( $\mathcal{C}_n$ , triangles) correlations.

and spin-orbital fluctuations are strong becomes broader by increasing cluster size from N6 to N10.

The clusters N6 and N10 do not have any spin degeneracy and total spin state is a singlet  $\mathcal{S} = 0$  in the entire parameter range. The degeneracy of N6 cluster (see Table I) follows therefore from the distribution of three spin singlets over the cluster accompanied by matching the orbital state in such a way, that the energy of these singlet states can indeed contribute to the GS energy.

TABLE I: Degeneracy of different GSs found in the  $d^1$  spin-orbital model Eq. (2.18) at the superexchange point ( $\alpha = 0$ ), at finite but small  $\alpha = \epsilon$ , in the intermediate regime ( $\alpha = 0.6$ ), close to  $(1 - \alpha = \epsilon)$  and at the direct exchange ( $\alpha = 1$ ) point for the triangular N3, N6 and N10 clusters shown in Fig. 2(a).

cluster	$\alpha = 0$	$\alpha = \epsilon$	$\alpha = 0.6$	$\alpha = 1 - \epsilon$	$\alpha = 1$
N3	6	4	2	8	12
N6	2	1	2	1	2
N10	1	2	1	2	6



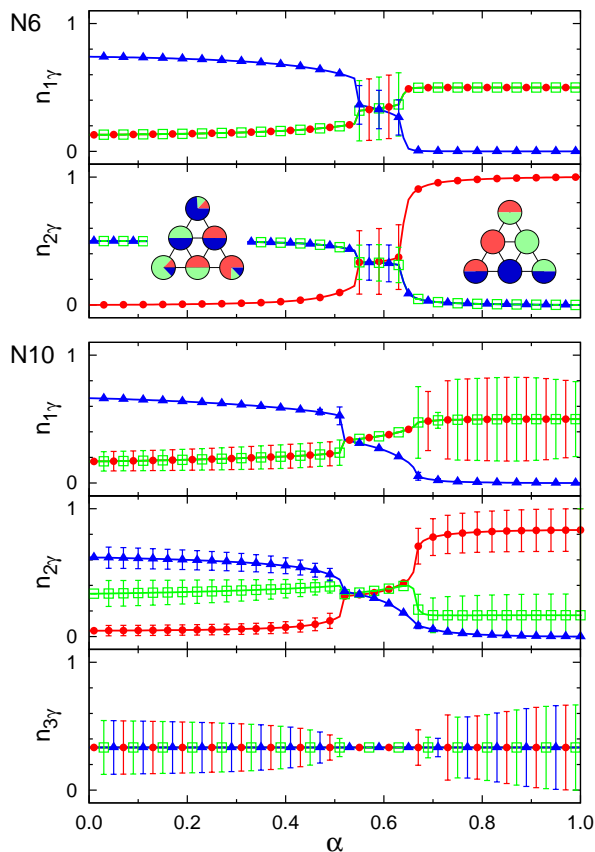


FIG. 5: (Color online) Orbital occupations  $n_{1\gamma}$  in triangular clusters for increasing  $\alpha$  in the absence of Hund's exchange ( $\eta = 0$ ): at sites  $i = 1, 2$  for N6 cluster (top), and sites  $i = 1, 2, 3$  for N10 cluster (bottom), see Fig. 2(a). Insets show two representative orbital occupancy distributions for the superexchange (left) and direct exchange (right) regime.

The overall tendency towards singlet spin correlations on the bonds originating from a corner site 1, see Fig. 2(a), is observed in both N6 and N10 clusters, where  $\mathcal{S}_1 < -0.12$  in the entire regime of  $\alpha$ . Gradual localization of spin singlets near corner sites with increasing  $\alpha$  is suggested by the decreasing values of  $\mathcal{S}_1$ , with the lowest values reached at  $\alpha = 1$  in both cases. The superexchange regime extends up to  $\alpha \simeq 0.54$  ( $\alpha \simeq 0.51$ ) for N6 (N10) cluster, while the direct exchange dominates for  $\alpha > 0.64$  ( $\alpha > 0.67$ ), respectively. A small increase of  $\mathcal{S}_1$  in N6 cluster for  $0 < \alpha < 0.54$  could be understood as a consequence of gradual increase of orbital fluctuations towards the intermediate regime, where spin and orbital dynamics start to decouple from each other. This trend is recognized from simultaneous decrease of spin correlations  $\mathcal{S}_1$  and increase of spin-orbital correlations  $\mathcal{C}_1$ . A common feature for both N6 and N10 clusters in the regime of large  $\alpha$  is vanishing spin-orbital correlation function ( $\mathcal{C}_1 = 0$ ), see Fig. 4.

We remark that also the correlations on bonds labeled as 2 in the clusters N6 and N10, see Fig. 2(a), have several common features. First, spin correlations are nega-

tive ( $\mathcal{S}_2 < 0$ ) in the entire range of  $\alpha$  except for  $\alpha = 1$ , where one finds  $\mathcal{S}_2 = 0$ . We argue that this result manifests frustration of the internal bonds (labeled 2) in both clusters in contrast to the bonds originating from a corner (labeled 1). Second, the orbital correlations  $\mathcal{T}_2$  are positive both for small and large values of  $\alpha$ , while in the intermediate regime these correlations are negative due to large orbital fluctuations. Finally, the spin-orbital correlations vanish on bonds 2 in both clusters when the direct exchange point  $\alpha = 1$  is approached. These results confirm the observations made above for the bonds 1 originating from a corner that spin-orbital entanglement is absent at the direct exchange point.

Three different regimes of spin and orbital correlations recognized in N6 and N10 clusters are characterized by quite different density distributions of electrons which obey the local constraint Eq. (2.2). The electron densities, shown in Fig. 5, confirm the observations made above by analyzing the intersite correlations that the GSs of both clusters can be classified as belonging to three different regimes dominated by: (i) the superexchange, (ii) orbital fluctuations, and (iii) direct exchange. Different role played by the orbitals  $\{a, b, c\}$  along particular directions in N6 cluster are highlighted by the two insets in Fig. 5. The bonds which originate at a corner site  $i = 1$  are remarkably similar to each other. The common active orbital  $c$  for the superexchange along both bonds has a large electron density, while the remaining orbitals may contribute only along one of these bonds. In the smaller N6 cluster the density distribution at  $\alpha = 0$  amounts to  $n_{1c} \simeq 0.74$  and  $n_{1a} = n_{1b} \simeq 0.13$ . This density distribution cannot be easily deduced by analyzing the degeneracy of the GS (Table I) and by averaging spin singlet configuration over the bonds in the N6 cluster which gives instead  $\{n_{1a}, n_{1b}, n_{1c}\} = \{1/6, 1/6, 2/3\}$ . Therefore, we find here the first example where the orbital fluctuations play a role and modify the electron density distribution with respect to the classical expectations. Nevertheless, the spin singlets are accompanied by appropriate active orbitals along three isolated bonds, each of them originating from one corner site of N6 triangle. This is also confirmed by the density distribution found for the site  $i = 2$ , where one finds the density of 0.5 for both orbitals active along the bonds on the triangle edge and 0 for the third orbital which contributes to the superexchange along the other two triangle edges. To some extent this is also observed in the larger N10 cluster.

The density distribution at sites  $i = 1$  and  $i = 2$  changes towards more isotropic one for increasing  $\alpha$ , but the symmetry in the orbital space is always broken by geometry and the densities differ somewhat even in the intermediate regime for  $\alpha \sim 0.6$  (Fig. 5). For larger values of  $\alpha$  one recognizes easily the situation of singlet spin dimers distributed over the cluster. Each dimer is based on a single orbital flavor active in the direct exchange on the particular bond. This state is surprisingly robust against orbital fluctuations in N6 cluster, where only the orbitals  $a$  and  $b$  are occupied at site  $i = 1$ , and

$n_{1a} = n_{1b} = 0.5$ . Actually, a similar situation is found also in N10 cluster, but here the GS is degenerate, see Table I, and a range of possible electron densities  $\{n_{1a}, n_{1b}\}$  is found instead. Altogether, we have found that  $n_{1c} = 0$  in all the considered triangular clusters when the direct exchange limit is approached.

The distribution of orbital densities at sites labeled  $i = 2$  in clusters N6 and N10 in the regime of large  $\alpha > 0.7$  demonstrates that indeed these clusters are dominated by the spin singlets touching a corner site each. It is for this reason that the density  $n_{2a}$  approaches  $n_{2a} = 1$  when  $\alpha \rightarrow 1$ , and the other two orbitals are empty. In N10 cluster the density  $n_{2a}$  is somewhat reduced due to the geometric constraints and additional frustration introduced by the total number of five spin singlets which implies several equivalent states with different orbital density distributions in the cluster.

The only site in the triangular clusters which recovers full symmetry in the orbital space is the central  $i = 3$  site of N10 cluster. Here we have found that all three orbitals contribute equally in the GS in the entire range of  $\alpha$ , with  $n_{3\gamma} = 1/3$  (Fig. 5), but certain fluctuations around this average value are observed both in the superexchange ( $\alpha < 0.52$ ) and direct exchange ( $\alpha > 0.66$ ) regime. This result may be treated as a precursor of the situation encountered in the infinite lattice, where the geometrical frustration favors the disordered state. Such an interpretation is also supported by the fact that the GS energies per bond (not shown) systematically increase with increasing cluster size (for fixed  $\alpha$ ) among N3, N6 and N10 clusters, particularly close to superexchange ( $\alpha = 0$ ) and direct exchange ( $\alpha = 1$ ) points. We shall investigate this situation in more detail below (in Sec. III C) by considering the clusters with PBC.

### C. Clusters with periodic boundary conditions

After analyzing the triangular clusters with OBC in Sec. III B, we turn to the clusters N4, N7 and N9 with PBC, shown in Fig. 2(b), which have all the sites equivalent and are thus representative for the triangular lattice in the thermodynamic limit. The intersite correlation functions obtained for N4 cluster were analyzed in Ref. 25, and we shall concentrate here on both larger clusters, N7 and N9.

Unlike for the triangular clusters where abrupt transitions between distinct regimes of particular spin and orbital correlations were found, one finds here that the intersite spin, orbital and spin-orbital correlations evolve continuously with increasing  $\alpha$  for N7 and N9 clusters, and no distinct regimes with dominating either superexchange or direct exchange can be identified. In case of N7 cluster the spin correlations are AF and constant,  $S_{ij} \simeq -0.11$ . Note that this value is somewhat higher than the average obtained by considering randomly distributed spin singlets over the triangular lattice, i.e., occupying every sixth bond in the lattice and leading to

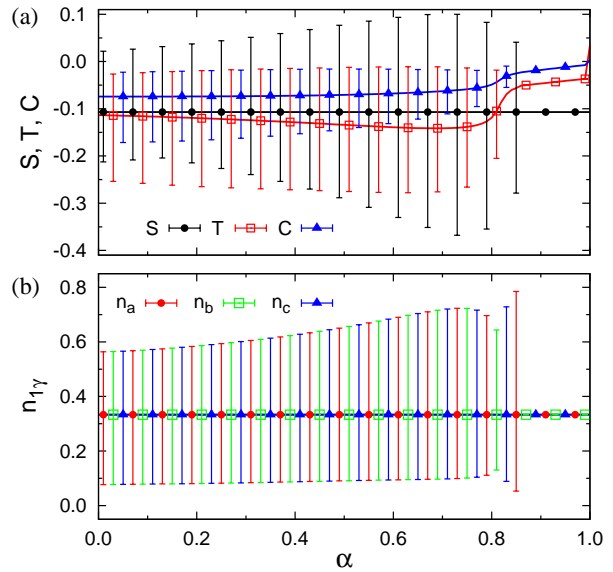


FIG. 6: (Color online) Evolution of the frustrated GS for N7 cluster with PBC shown in Fig. 2(b) with increasing  $\alpha$  in the absence of Hund's exchange: (a) intersite bond correlations — spin ( $S_{ij}$ , circles), orbital ( $T_{ij}$ , squares), and spin-orbital ( $C_{ij}$ , triangles); (b) orbital occupations  $n_{1\gamma}$  per site (at a representative site  $i = 1$ ).

$\langle S_{ij} \rangle = -0.125$ . However, the obtained smaller value can be justified as follows. In the low-spin phase one has  $\mathcal{S} = 1/2$  total spin, and one can determine the intersite spin correlations using the following identity:

$$\mathcal{S}^2 = 7\bar{S}_i^2 + 42\langle \vec{S}_i \cdot \vec{S}_j \rangle. \quad (3.1)$$

For this cluster every pair of sites  $\{i, j\}$  is a nearest neighbor pair and forms a bond (due to PBC), so Eq. (3.1) follows. The value  $\langle \vec{S}_i \cdot \vec{S}_j \rangle = -3/28 = -0.107$  obtained from it is much reduced from the classical AF spin correlations  $-1/4$  in the Néel state on a square lattice, which is a consequence of high frustration of the triangular lattice. Note that spin correlations are here substantially reduced by the geometrical frustration, and seem not to be further hindered by orbital fluctuations, unlike in the 1D SU(4) model,<sup>33</sup> where the coupling to the orbital correlations is crucial and reduces spin correlations although the geometrical frustration is absent.

For the values of  $\alpha < 0.8$  the orbital correlations  $T_{ij}$  are even a bit lower than the spin ones, and decrease somewhat with increasing  $\alpha$  for  $\alpha < 0.6$ . We emphasize that both spin and orbital correlations are here negative, so the present spin-orbital model on the triangular lattice violates the Goodenough-Kanamori rules that these correlations should be complementary.<sup>34</sup> This is also reflected in the finite spin-orbital correlations  $C_{ij} \simeq -0.07$  which indicate that entangled states play an important role in this parameter range, see Fig. 6. When  $\alpha$  increases further, however, the orbital state is reorganized and the orbital correlations rapidly decrease. At the

same time the mixed spin-orbital correlations also decrease suggesting gradual disentanglement of spin and orbital degrees of freedom. Finally, at  $\alpha = 1$  the spins decouple from the orbitals, which agrees with the GS consisting of uncoupled spin singlets distributed over the triangular lattice.<sup>26</sup>

As all the orbitals are equivalent, the average occupancy is  $n_{i\gamma} = 1/3$ , see Fig. 6. However, apart from the spin degeneracy due to the total spin state  $\mathcal{S} = 1/2$  realized for the cluster with odd  $N = 7$  sites, one finds that several equivalent orbital configurations contribute, with one of the orbitals occupied by three electrons and the other two by two each. For this reason we have found degeneracy  $d = 6 \times 2 = 12$ , see Table II and large fluctuations of the density distribution, typically between 0.1 and 0.6 for low values of  $\alpha < 0.5$ , and increasing towards  $\alpha = 0.85$ . Next the quantum nature of the GS makes it only spin degenerate and  $d = 2$  for  $\alpha > 0.85$  and no fluctuations in the orbital occupancies were found. Finally, in the direct exchange limit  $\alpha = 1$  independent dimer distributions over the cluster dominate and determine large orbital degeneracy  $d = 147 \times 2$  of the GS. This degeneracy due to the orbital distribution over the cluster can be understood as given by 3 possibilities of having one dominating orbital flavor, 7 positions of this extra flavor in the cluster, and 7 possible distributions of singlets over the cluster, i.e.,  $3 \times 7 \times 7 = 147$ .

The second cluster with PBC contains  $N = 9$  sites and is better designed to study the present model as the degeneracy of the GS is expected to be lower (except at  $\alpha = 1$ ). In this case electrons can be equally distributed over the orbitals, and three electrons occupy each of them. Fluctuations over different values of bond orbital correlations  $T_{ij}$  and differently occupied orbital states, see Figs. 7(a) and 7(b), cannot be avoided within the cluster, but they are typically smaller than those found for N7 cluster. All average values for the intersite correlations are rather similar to those found in N7 cluster for small  $\alpha$ , with  $S_{ij} \simeq -0.90$ ,  $T_{ij} \simeq -0.97$ , and  $C_{ij} \simeq -0.64$  at  $\alpha = 0$ . Here all the orbital states are equally populated as shown by the inset in Fig. 7, but undergo local fluctuations, seen both in the intersite cor-

TABLE II: Degeneracy  $d$  of the GSs found for the  $d^1$  spin-orbital model Eq. (2.18) at the superexchange point ( $\alpha = 0$ ), in the intermediate regime ( $0 < \alpha < 1$ ) and at the direct exchange point ( $\alpha = 1$ ) obtained for N7 and N9 clusters with PBC. The first factor in  $d$  gives the orbital degeneracy which is multiplied by spin degeneracy 2 for the GS with  $\mathcal{S} = 1/2$  total spin.

cluster	N7	N9
$0 \leq \alpha < 0.26$	$6 \times 2$	$6 \times 2$
$0.26 < \alpha < 0.41$	$6 \times 2$	$4 \times 2$
$0.41 < \alpha < 0.85$	$6 \times 2$	$2 \times 2$
$0.85 < \alpha < 1$	$1 \times 2$	$6 \times 2$
$\alpha = 1$	$147 \times 2$	$756 \times 2$

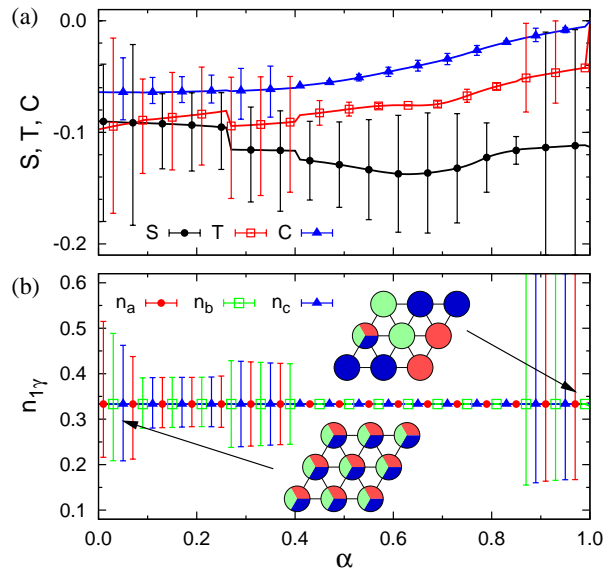


FIG. 7: (Color online) Evolution of the frustrated GS for N9 cluster with PBC shown in Fig. 2(b) with increasing  $\alpha$  in the absence of Hund's exchange: (a) intersite bond correlations — spin ( $S_{ij}$ , circles), orbital ( $T_{ij}$ , squares), and spin-orbital ( $C_{ij}$ , triangles); (b) orbital occupations  $n_{1\gamma}$  per site (at a representative site  $i = 1$ ). Insets show typical orbital patterns in the superexchange ( $\alpha = 0$ ) limit and direct exchange ( $\alpha = 1$ ) limit.

relation functions  $\{S_{ij}, T_{ij}, C_{ij}\}$  and in the electron densities  $\{n_{ia}, n_{ib}, n_{ic}\}$ .

The range of fluctuations in bond correlations is reduced but stays finite up to  $\alpha \simeq 0.41$ . Here the orbital degeneracy of the GS is first 6 up to  $\alpha = 0.26$ , and next drops to 4, see Table II. This regime is followed by a qualitatively new situation in the intermediate regime of  $\alpha$  values (compared to N7 cluster), with no fluctuations in the orbital distribution when  $0.41 < \alpha < 0.85$ . This regime is characterized by low degeneracy 2 in the orbital space. In this case the orbitals undergo strong local quantum fluctuations but their distribution in the cluster does not change, as seen in the stable density distribution, with  $n_{1\gamma} = 1/3$ . This regime can be identified as dominated by orbital fluctuations due to the mixing terms  $\mathcal{H}_m$  Eq. (2.17), with gradual suppression of spin-orbital fluctuations under increasing  $\alpha$  seen in the reduced values of  $|C_{ij}|$ .

Finally, when the orbital mixing terms sufficiently decrease, one finds that both spin and orbital correlations fluctuate stronger above  $\alpha = 0.85$  which follows from a random electron distribution over the available orbital states. In contrast to the superexchange regime with equally distributed electrons over the orbital flavors, the representative state shown in the inset in Fig. 7, is dominated by  $c$  orbitals. Equivalent configurations can be obtained by cyclic permutations of the density distribution in the  $\{a, b, c\}$  orbitals, and changing favored dimer direction in the cluster. For this reason degeneracy of

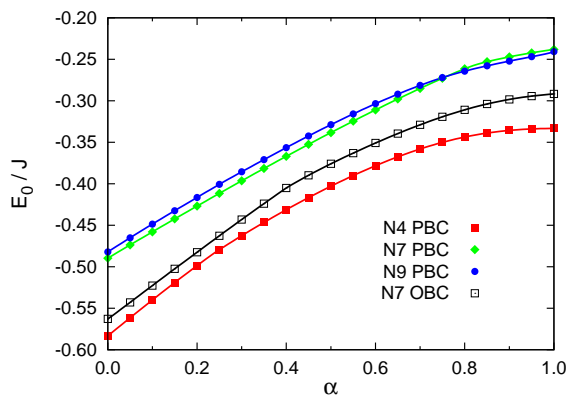


FIG. 8: (Color online) Ground state energy  $E_0$  per bond for clusters N4 (filled squares), N7 (diamonds), and N9 (circles) with PBC conditions for increasing  $\alpha$ . For a comparison the result obtained for N7 cluster with OBC is shown by empty squares. Parameter:  $\eta = 0$ .

the GS increases by a factor of 3, reflecting three possible with states dominated by one orbital flavor, see Table II. The direct exchange limit is again special, and characterized by large orbital degeneracy 756.

The GS energies obtained for N4, N7 and N9 clusters with the PBC (Fig. 8) exhibit a monotonous increase with increasing  $\alpha$ . The energy is the lowest for the smallest N4 cluster, and increases when the cluster size is increased to N7 or N9, indicating frustrated interactions. However, the energies obtained for N7 or N9 clusters are very close to each other which we take as an evidence that these clusters are already representative for the situation in the thermodynamic limit. We remark that the energy obtained for N7 cluster with OBC is lower than that found for the same cluster size with PBC which is again consistent with strongly frustrated spin-orbital interactions on the triangular lattice. This resembles the situation in spin systems with frustrated interactions, where one expects that clusters with OBC would give lower energy per bond than the ones with PBC as then additional breaking of symmetry is possible in the GS.

#### IV. THE MODEL AT LARGE HUND'S EXCHANGE

##### A. Orbital model for the FM phase

Until now we considered the spin-orbital model Eq. (2.3) in the regime of no Hund's exchange,  $\eta = 0$ . Finite Hund's exchange is responsible for the competition of FM with AF spin interactions in the perovskite Mott insulators described by similar spin-orbital models, and the orbital order is usually modified in a particular way. Well known examples are the *A*-AF phase in  $\text{LaMnO}_3$ ,<sup>16</sup> or *C*-AF phase in  $\text{LaVO}_3$ .<sup>21</sup> The present and earlier<sup>25</sup>

study of the spin-orbital  $d^1$  model on the triangular lattice, however, suggest that orbital disorder is favored in this geometrically frustrated lattice. Having no orbital order excludes *de facto* an intermediate phase (at intermediate values of  $\eta$ ) with coexisting FM and AF interactions in the present case. This is confirmed by the exact diagonalization of finite clusters, at least in the considered case when all the interactions along three bond directions are equivalent. Thus, there are two problems to be addressed in the theory: (i) the nature of orbital correlations in the FM phase in the range of large values of  $\eta$ , and (ii) the phase diagram in the  $(\alpha, \eta)$  plane. The first of these questions is easier to answer and we consider it below, the second one will be discussed in Secs. IV B and V.

The exchange interactions in  $\mathcal{H}$  given by Eq. (2.3) simplify in the FM phase, when only excitations to high-spin states contribute and all the low-spin terms vanish, i.e.,  $\langle \vec{S}_i \cdot \vec{S}_j - \frac{1}{4} \rangle \equiv 0$ . The Hamiltonian reduces then to the orbital model,

$$\begin{aligned} \mathcal{H}_{\text{orb}} = & -\frac{1}{4} J r_1 \sum_{\langle ij \rangle \| \gamma} \left\{ -(1-\alpha) \left[ 2A_{ij}^{(\gamma)} + (n_{i\gamma} + n_{j\gamma}) - 2 \right] \right. \\ & + \sqrt{\alpha(1-\alpha)} \left( T_{i\mu}^+ T_{j\nu}^+ + T_{i\nu}^+ T_{j\mu}^+ + T_{i\nu}^- T_{j\mu}^- + T_{i\mu}^- T_{j\nu}^- \right) \\ & \left. + \alpha \left[ n_{i\gamma}(1 - n_{j\gamma}) + (1 - n_{i\gamma})n_{j\gamma} \right] \right\}. \end{aligned} \quad (4.1)$$

In the superexchange regime ( $\alpha \simeq 0$ ) it favors pairs of different orbitals, both not oriented along the considered bond, and in the direct exchange regime ( $\alpha \simeq 1$ ) — pairs of different orbitals, one oriented along the bond and the other not.

Complete information about the orbital correlations in the parameter regime where the FM phase is stable may be obtained by considering the following orbital projection operators for a bond  $\langle ij \rangle \| \gamma$ :

$$P_{ij}^{(\gamma)} = \langle n_{i\gamma} n_{j\gamma} \rangle, \quad (4.2)$$

$$Q_{ij}^{(\gamma)} = \langle n_{i\gamma}(1 - n_{j\gamma}) \rangle + \langle (1 - n_{i\gamma})n_{j\gamma} \rangle, \quad (4.3)$$

$$R_{ij}^{(\gamma)} = \langle (1 - n_{i\gamma})(1 - n_{j\gamma}) \rangle. \quad (4.4)$$

Here the operator  $n_{i\gamma}$  stands for the electron density in the orbital oriented along the bond  $\langle ij \rangle$  at site  $i$ , while  $(1 - n_{i\gamma})$  is the complementary electron density in the two remaining orbitals, as given by the local constraint Eq. (2.2). The above projection operators may be treated as probabilities to encounter a given orbital configuration, and they obey the usual condition,

$$P_{ij}^{(\gamma)} + Q_{ij}^{(\gamma)} + R_{ij}^{(\gamma)} = 1. \quad (4.5)$$

Knowing these probabilities allows us for a complete characterization of the orbital state on a representative bond  $\langle ij \rangle \| c$ .

First we present distinct differences between the distribution of occupied orbitals between the superexchange ( $\alpha \simeq 0$ ) and direct exchange ( $\alpha \simeq 1$ ) regime found for

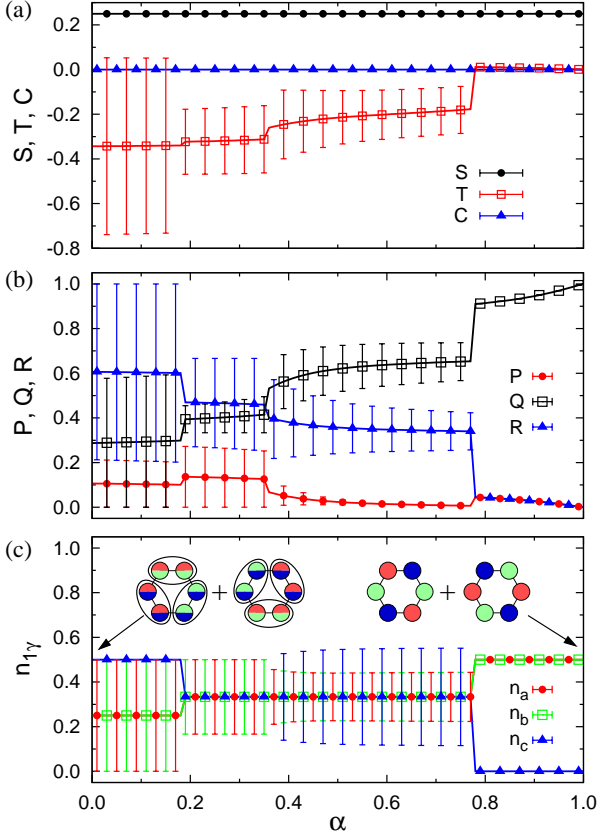


FIG. 9: (Color online) Evolution of the orbital state in the FM GS of the hexagonal H6 cluster with OBC, as found at large  $\eta = 0.2$  for increasing  $\alpha$ : (a) spin  $S \equiv S_{ij}$ , orbital  $T \equiv T_{ij}$  and spin-orbital  $C \equiv C_{ij}$  bond correlations; (b) orbital bond projection operators  $P \equiv P_{ij}^{(\gamma)}$  (circles),  $Q \equiv Q_{ij}^{(\gamma)}$  (squares), and  $R \equiv R_{ij}^{(\gamma)}$  (triangles); (c) orbital electron densities  $n_{1\gamma}$  on the most left cluster site  $i = 1$ . Insets in (c) show two equivalent states in the superexchange ( $\alpha = 0$ ) and direct exchange ( $\alpha = 1$ ) limit.

the FM hexagonal H6 cluster. Here the orbital bond correlations change from  $T_{ij} \simeq -0.34$  at  $\alpha = 0$  to  $T_{ij} \simeq 0$  at  $\alpha = 1$ , while the spins are FM ( $S_{ij} = 0.25$ ) and disentangled from the orbital state ( $C_{ij} = 0$ ), see Fig. 9(a). This latter feature is common for FM states in other clusters as well (see below) and the Goodenough-Kanamori rule<sup>34</sup> is obeyed, i.e., FM spin correlations are accompanied by negative orbital correlations which indicate that orbitals show a tendency towards alternating orbital order.

The FM state in the superexchange regime ( $\alpha \simeq 0$ ) is stabilized by pairs of orbitals which do not include the one oriented along the considered bond. This is indicated by the inset in Fig. 9(c), where two possible configurations with pairs of active orbitals on the bonds of H6 cluster, forming almost orbital singlets, are shown. In this case the largest average projection operator is  $\langle R_{ij}^{(\gamma)} \rangle$ , see Fig. 9(b), and the orbital density is the largest for the  $c$  orbital which participates in the singlets for both possible

cluster coverings, i.e.,  $n_{1c} = 0.5$  and  $n_{1a} = n_{1b} = 0.25$ .

The intermediate regime extends in the FM H6 cluster from  $\alpha = 0.19$  to  $\alpha = 0.77$ , where the orbital densities are the same in each orbital,  $n_{1\gamma} = 1/3$ , see Fig. 9(c). However, the orbital correlations on the bonds are not constant, but gradually change towards pairs of one  $\gamma$  orbital accompanied by a different orbital on each bond  $\langle ij \rangle \parallel \gamma$  with increasing  $\alpha$ , as depicted by the projection operator  $\langle Q_{ij}^{(\gamma)} \rangle$  in Fig. 9(b). Simultaneously the orbital correlation  $T_{ij}$  is gradually reduced. Finally, for  $\alpha > 0.77$  the orbital distribution changes to pairs of orbitals, one oriented along the bond and the other not, favored in the direct exchange regime. Once again, there are two possible distributions of orbitals over the H6 cluster, and this gives for site  $i = 1$  two contributing densities:  $n_{1a} = n_{1b} = 0.5$ , while the orbital which participates in the direct exchange only on two horizontal bonds is empty, i.e.,  $n_{1c} = 0$ , see Fig. 9(c).

The above transparent picture of the occupied orbitals in different  $\alpha$  regimes for H6 cluster is strongly modified in the GS of the symmetric N7 cluster by frustration of spin-orbital interactions and by the absence of symmetry breaking in the orbital space due to the PBC, see Fig. 10. At  $\alpha = 0$  one finds negative orbital correlation function  $T_{ij} \simeq -0.23$ , see Fig. 10(a). The orbital correlations are quite well developed here as they are not hindered by spin fluctuations, as it was the case at  $\eta = 0$  (Fig. 6). With increasing  $\alpha$  the orbital correlations are gradually reduced, and reach the limiting value  $T_{ij} = -0.0357$  at  $\alpha = 1$  which corresponds to randomly distributed dimers consisting of a pair of active and inactive orbital in the direct exchange over the bonds of N7 cluster.

Two distinct regimes: one with fluctuating values of  $T_{ij}$  for  $\alpha < 0.85$ , and the other one with uniquely determined  $T_{ij}$  for  $\alpha > 0.85$  correspond to the degenerate and nondegenerate GS of the N7 cluster, respectively. Similar fluctuating results for the average projection operators  $\{P_{ij}^{(\gamma)}, Q_{ij}^{(\gamma)}, R_{ij}^{(\gamma)}\}$  and for the orbital densities  $\{n_{1a}, n_{1b}, n_{1c}\}$  were found in the range of  $\alpha < 0.85$ , see Figs. 10(b) and 10(c). In the regime of small  $\alpha < 0.4$  configurations with two orbitals active in the superexchange processes are the most probable ones, i.e.,  $R_{ij}^{(\gamma)} > P_{ij}^{(\gamma)}$  and  $R_{ij}^{(\gamma)} > Q_{ij}^{(\gamma)}$ . On the contrary, when  $\alpha > 0.4$ , pairs of orbitals, one active and the other one inactive in the direct exchange processes, dominate, i.e.,  $Q_{ij}^{(\gamma)} > R_{ij}^{(\gamma)}$  and  $P_{ij}^{(\gamma)} \rightarrow 0$  when  $\alpha \rightarrow 1$ . Here the results suggest a single quantum state with equally distributed orbital flavors over the cluster,  $n_{1\gamma} = 1$ .

We have verified that the above evolution of the orbital state in N7 cluster is representative for the present triangular lattice in the FM regime by considering two larger clusters with PBC (not shown): (i) N12 cluster obtained by adding 5 sites to N7, e.g. on the right hand side and on top, and (ii) a star-like N13 cluster obtained by adding a triangle to each side of N7 cluster. Both clusters have all sites equivalent and may be used to cover the lattice (in the second case two equivalent coverings differ

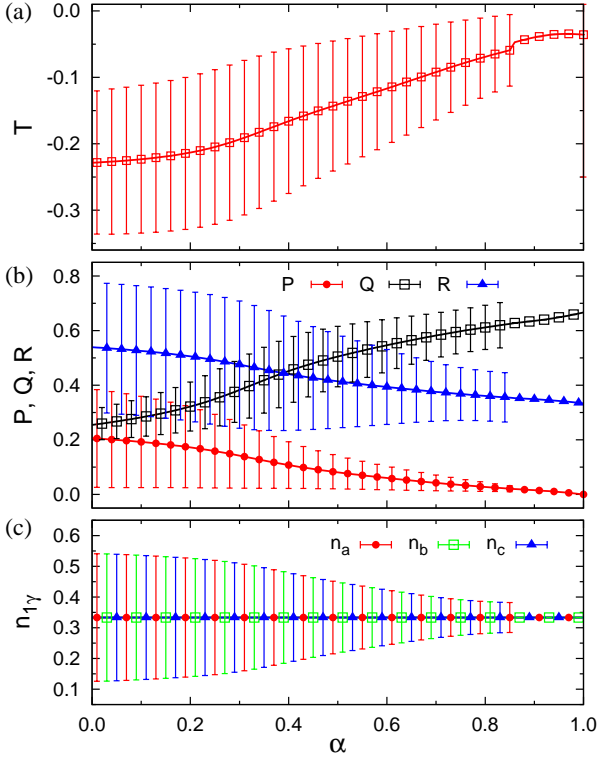


FIG. 10: (Color online) Evolution of the orbital state in the FM GS of N7 cluster for increasing  $\alpha$ , found with PBC at large  $\eta = 0.2$ : (a) bond orbital correlations  $T \equiv T_{ij}$ ; (b) orbital occupation correlations  $P \equiv P_{ij}^{(\gamma)}$  (circles),  $Q \equiv Q_{ij}^{(\gamma)}$  (squares), and  $R \equiv R_{ij}^{(\gamma)}$  (triangles); (c) orbital electron densities  $n_{1\gamma}$ .

by chirality). In both cases we found that the orbital bond correlations  $T_{ij}$  increase from  $T_{ij} \simeq -0.23$  at  $\alpha = 0$  to  $T_{ij} \simeq 0$  at  $\alpha = 1$ . The occupied orbitals give again (as for N7) large  $R_{ij}^{(\gamma)} \simeq 0.5$  at the superexchange limit  $\alpha = 0$ . It decreases with increasing  $\alpha$ , and one finds instead large  $Q_{ij}^{(\gamma)} \simeq 2/3$  at the direct exchange case  $\alpha = 1$ . Interestingly, the orbital fluctuations shown by the vertical lines are reduced in both cases, and they do not occur at all in N12 cluster both for  $\alpha < 0.62$  and for  $\alpha > 0.81$ .

## B. Phase diagrams

Perhaps the most intriguing question concerning the GS of the spin-orbital model Eq. (2.3) is the phase diagram and the way the FM state occurs as a function of both model parameters,  $\alpha$  and  $\eta$ . Having no possibility to access the phase diagram in the thermodynamic limit (see also Sec. V), we shall concentrate here on a few representative clusters trying to extract the common and generic features of the low-to-high spin transition.

The hexagonal H6 cluster, with low-spin and high-spin states shown in Figs. 3 and 9, serves here as an example of unfrustrated geometry. The transition to the high-

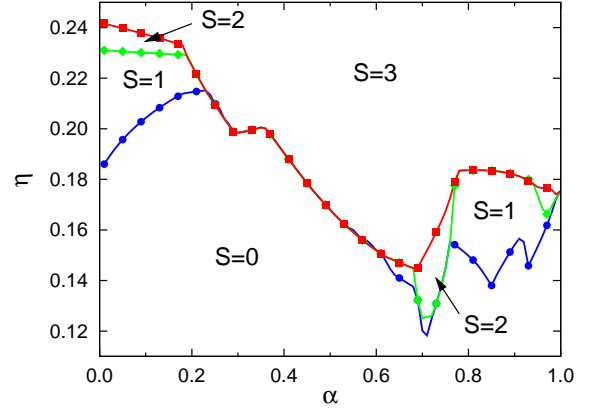


FIG. 11: (Color online) Phase diagram in the  $(\alpha, \eta)$  plane as obtained for the hexagonal H6 cluster with OBC. The total spin of the GS is indicated in the transition regime from the singlet phase ( $S = 0$ ) to the high-spin ( $S = 3$ ) phase.

spin  $S = 3$  state is then gradual and passes through intermediate  $S = 1$  and (in some cases)  $S = 2$  states when  $\alpha$  is close to 0 or 1, see Fig. 11. In contrast, for the intermediate values of  $0.22 < \alpha < 0.62$  the transition takes place directly between the  $S = 0$  and  $S = 3$  states. We recall that in the regime of intermediate  $\alpha$  values orbital fluctuations play an important role, and they also couple to spin fluctuations. Therefore, this behavior in the phase diagram reflects the stabilizing role of the joint spin-orbital fluctuations in the singlet phase,  $S = 0$ . When spin value increases, such fluctuations are partly damped and therefore intermediate spin values are here not realized.

An interesting result was obtained for H6 cluster in the superexchange regime (at  $\alpha \simeq 0$ ). Here the transition from the singlet to the  $S = 1$  state occurs at  $\eta = 0.186$ . It is followed by the transition to the  $S = 2$  state at  $\eta = 0.231$ , and the final transition to the spin-polarized  $S = 3$  state takes place only at  $\eta = 0.242$ . Here the phases with intermediate spin values arise as a consequence of spin fluctuations that stabilize them in between the low-spin and high-spin states. A similar situation was found close to but not at the direct exchange point  $\alpha = 1$ . In fact, spin fluctuations in the direct exchange limit concern only pairs of spins in the singlet  $S = 0$  phase, so a singlet-triplet transition for a single bond induces here the global transition to the  $S = 3$  phase. Altogether, the transition to the high-spin phase occurs here at  $\eta_c \simeq 0.188$ , in agreement with the classical expectation, see also Eq. (5.10) in Sec. V, and this critical value is enhanced in the superexchange dominated regime due to spin-orbital fluctuations which are here stronger in the singlet phase.

The phase diagrams obtained for three triangular clusters, N3, N6, and N10, are shown in Fig. 12. As for the hexagonal H6 cluster, the transition to the high-spin phase occurs for  $\eta \simeq 0.18$ , but the critical value of  $\eta$

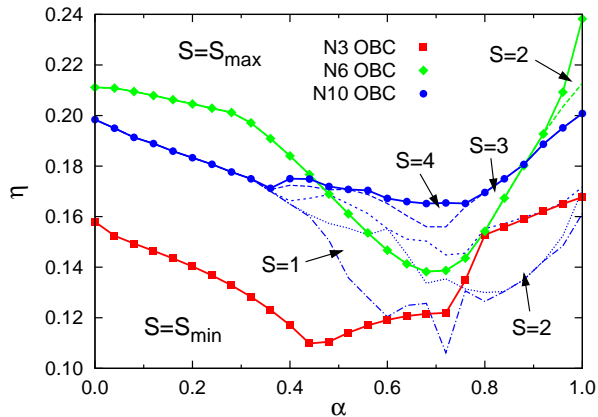


FIG. 12: (Color online) Phase diagram in the  $(\alpha, \eta)$  plane as obtained for triangular clusters with OBC: N3 (squares),<sup>35</sup> N6 (diamonds) and N10 (circles). The phase diagrams of N6 and N10 clusters contain also intermediate spin phases and the corresponding phase boundaries are shown as dashed lines (for the N6 cluster only near  $\alpha = 1$ ).

is larger for two bigger clusters (N6 and N10) than for the smallest N3 triangular cluster.<sup>35</sup> One finds here once again a signature of the stabilizing role played by orbital fluctuations in the low-spin phase. Particularly in the regime dominated by the superexchange, the onset of the high-spin phase occurs at values of  $\eta$  which are higher than at  $\alpha \simeq 0.5$  and increase from N3 ( $\eta = 0.158$ ) to larger clusters ( $\eta = 0.211$  and  $\eta = 0.198$  for N6 and N10 clusters). In all three cases the transition occurs to the phases with maximal spin and no intermediate phases in between.

Phases with intermediate spin values occur for two larger triangular clusters in the intermediate and direct exchange regime. We suggest that they are stabilized by orbital fluctuations which can couple to only partly polarized spin subsystem and provide certain energy gain. While this feature is general, the actual range of stability of the phases with intermediate spin values depends on the cluster size. At  $\alpha = 1$  one finds for N6 a transition to  $S = 3$  phase at a rather large value of  $\eta = 0.238$ , which demonstrates here particular stability of states with lower spin values, where more energy can be gained due to quantum fluctuations for certain orbital arrangements. However, in a larger N10 cluster this transition occurs at a lower value of  $\eta = 0.202$ .

When the phase diagrams obtained for the triangular clusters (Fig. 12) are compared with those for the clusters N7 and N9 with PBC (Fig. 13), one finds that the transition to the high-spin states occurs in general for somewhat lower values of  $\eta$  in the latter case. An extreme case here is N4 cluster with PBC, where a rather small value of  $\alpha \simeq 0.02$  suffices to destabilize the singlet phase at  $\alpha = 0$ . This peculiar result follows from the small size of this cluster which allows one to accommodate only two spin singlets when the orbital state is constrained to the pairs of orbitals supporting the superexchange processes,

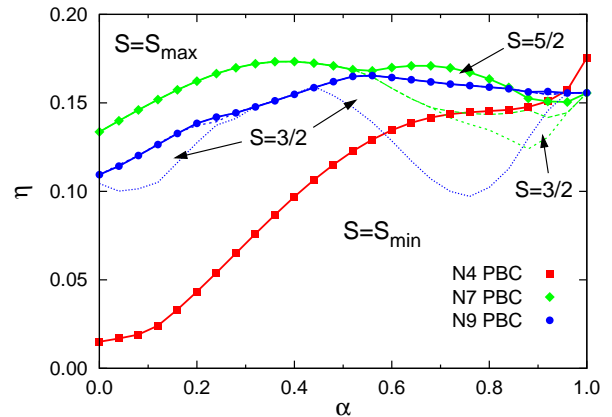


FIG. 13: (Color online) Phase diagram in the  $(\alpha, \eta)$  plane as obtained for clusters with PBC: N4 (squares),<sup>36</sup> N7 (diamonds) and N9 (circles). Ranges of stability of intermediate spin phases for N7 and N9 clusters are shown by thin lines and arrows.

while in the high-spin  $S = 2$  state these constraints are released and the orbital fluctuations of different kind stabilize it. In contrast, a similar critical value in the range of  $0.15 < \eta < 0.175$  is found for the low-to-high spin transition in all the clusters N4, N7, and N9 with PBC at  $\alpha = 1$ . This common feature which is almost independent of the cluster size suggests that static dimer configurations dominate in this case not only for the low-spin phase,<sup>26</sup> but also for the high-spin phase, where pairs of different orbitals are stable on individual bonds, see Fig. 10.

The proximity of critical values of  $\eta$  found for N7 and N9 clusters is very encouraging and suggests that one may expect the FM phase for  $\eta > 0.16$  in the thermodynamic limit, independently of the ratio of superexchange to direct exchange (i.e., on the actual value of  $\alpha$ ). In both clusters we have also found a range of stability for the phases with intermediate value of total spin which suggests that this transition is likely to be continuous, via weakly polarized FM states, also in the thermodynamic limit. It is remarkable, however, that intermediate spin states do not occur for the direct exchange interactions at  $\alpha = 1$  which demonstrates once again that quantum fluctuations do not play an important role in this case, and simple configurational averaging over available orbital dimer configurations on the lattice suffices to understand the magnetic transition described here.

## V. SPIN-ORBITAL ENTANGLEMENT

### A. Disentangled spin-orbital interactions

When analyzing the phase diagrams for the clusters with PBC, we have emphasized the role played by orbital and spin-orbital fluctuations, as well as spin-orbital

entanglement in the GS. Now we shall present additional data to support this claim. In order to address this question we introduce an approximate treatment of the spin-orbital Hamiltonian which uses MF decoupling of spin and orbital variables on the bonds.<sup>38</sup> Focusing on the magnetic interactions which concern here  $S = 1/2$  quantum spins coupled by the SU(2) symmetric interaction, we rewrite the  $d^1$  spin-orbital model Eq. (2.3) in a general form,<sup>23</sup>

$$\mathcal{H} = \sum_{\langle ij \rangle \| \gamma} \left\{ \hat{\mathcal{J}}_{ij}^{(\gamma)} \left( \vec{S}_i \cdot \vec{S}_j \right) + \hat{\mathcal{K}}_{ij}^{(\gamma)} \right\}, \quad (5.1)$$

where the operators  $\hat{\mathcal{J}}_{ij}^{(\gamma)}$  and  $\hat{\mathcal{K}}_{ij}^{(\gamma)}$  contain orbital pseudospin operators for a bond  $\langle ij \rangle$  along the direction  $\gamma$ . This form is helpful as one can deduce the values of spin exchange constants directly from it when the orbital operators are replaced by their averages in a particular (ordered or disordered) state. In particular, it helped to understand the origin of magnetic interactions in LaMnO<sub>3</sub>,<sup>16</sup> where such a decoupling scheme may be well justified and gives predictions for the optical spectral weights<sup>23</sup> that agree with the experimental data.<sup>37</sup>

Here we introduce the MF procedure to simplify Eq. (5.1) as follows,

$$\begin{aligned} \mathcal{H}_{\text{MF}} &= \sum_{\langle ij \rangle \| \gamma} \langle \hat{\mathcal{J}}_{ij}^{(\gamma)} \rangle \left( \vec{S}_i \cdot \vec{S}_j \right) \\ &+ \sum_{\langle ij \rangle \| \gamma} \left\{ \hat{\mathcal{J}}_{ij}^{(\gamma)} \langle \vec{S}_i \cdot \vec{S}_j \rangle + \hat{\mathcal{K}}_{ij}^{(\gamma)} \right\} \\ &- \sum_{\langle ij \rangle \| \gamma} \langle \hat{\mathcal{J}}_{ij}^{(\gamma)} \rangle \langle \vec{S}_i \cdot \vec{S}_j \rangle. \end{aligned} \quad (5.2)$$

The first term in Eq. (5.2) is the spin model as introduced in Ref. 23, the second one is a purely orbital model, while the last one is a double counting correction term for the spin-orbital part of the Hamiltonian Eq. (5.1). As an example we consider the orbital operator  $\hat{\mathcal{J}}_{ij}^{(c)}$  which stands as a coefficient of the Heisenberg spin interaction for a bond  $\langle ij \rangle$  along the  $c$  axis,

$$\begin{aligned} \hat{\mathcal{J}}_{ij}^{(c)} &= J(1-\alpha) \left\{ \frac{r_1 - r_2}{2} \left[ \frac{1}{2} (n_{ic} + n_{ic}) - 1 \right] \right. \\ &+ \frac{r_1 + r_2}{2} \left( T_{ic}^+ T_{jc}^+ + T_{ic}^- T_{jc}^- - 2T_{ic}^z T_{jc}^z + \frac{1}{2} n_i^{(c)} n_j^{(c)} \right) \\ &- \frac{r_2 - r_3}{2} \left( T_{ic}^+ T_{jc}^- + T_{ic}^- T_{jc}^+ - 2T_{ic}^z T_{jc}^z + \frac{1}{2} n_i^{(c)} n_j^{(c)} \right) \left. \right\} \\ &+ J\sqrt{\alpha(1-\alpha)} \frac{r_2 - r_1}{4} \left( T_{ia}^+ T_{jb}^+ + T_{ib}^- T_{ja}^- \right. \\ &\quad \left. + T_{ib}^+ T_{ja}^+ + T_{ia}^- T_{jb}^- \right) \\ &+ J\alpha \left\{ \frac{r_2 - r_1}{4} [n_{ic} (1 - n_{jc}) + (1 - n_{ic}) n_{jc}] \right. \\ &\quad \left. + \frac{2r_2 + r_3}{3} n_{ic} n_{jc} \right\}. \end{aligned} \quad (5.3)$$

The operators for the bonds along two other lattice directions can be obtained by permutations of  $\{a, b, c\}$  orbital indices. However, as all the bonds are equivalent, it suffices to consider the above operator  $\hat{\mathcal{J}}_{ij}^{(c)}$  for a representative bond to derive the exchange constant by averaging the orbital operators over the GS wave function  $|\Phi_0\rangle$ ,

$$J_{\text{MF}} \equiv \langle \Phi_0 | \hat{\mathcal{J}}_{ij}^{(\gamma)} | \Phi_0 \rangle. \quad (5.4)$$

Here the orbital fluctuation operators in the term  $\propto \sqrt{\alpha(1-\alpha)}$  contribute and couple different components of the wave function  $|\Phi_0\rangle$ .

We also consider a simplified classical quantity,

$$J_{\text{MF}}^0 \equiv \sum_n \langle n | \hat{\mathcal{J}}_{ij}^{(\gamma)} | n \rangle |\langle n | \Phi_0 \rangle|^2, \quad (5.5)$$

where the summation includes basis states  $\{|n\rangle\}$  with all possible orbital configurations in the considered cluster. As the basis states are used for calculating the average in Eq. (5.5) which is the same along all the bonds. This result may be derived from Eq. (5.3) by neglecting the orbital dynamics, *inter alia* the terms  $\propto \sqrt{\alpha(1-\alpha)}$ , and keeping only the diagonal orbital terms. One finds then the approximate form of the spin interaction,

$$\begin{aligned} \bar{\mathcal{J}}_{ij}^{(c)} &= J(1-\alpha) \left\{ -\frac{3r_1 + r_2 + 2r_3}{3} \left( T_{ic}^z T_{jc}^z - \frac{1}{4} n_i^{(c)} n_j^{(c)} \right) \right. \\ &\quad \left. + \frac{r_1 - r_2}{4} (n_{ic} + n_{jc} - 2) \right\} \\ &+ J\alpha \left\{ \frac{r_2 - r_1}{4} [n_{ic} (1 - n_{jc}) + (1 - n_{ic}) n_{jc}] \right. \\ &\quad \left. + \frac{2r_2 + r_3}{3} n_{ic} n_{jc} \right\}. \end{aligned} \quad (5.6)$$

Further simplification follows from an observation that for uniform electron distribution in the spin-orbital liquid state one finds the following averages for the relevant density and pseudospin operators:

$$\langle n_{i\gamma} \rangle = \frac{1}{3}, \quad \langle n_i^{(\gamma)} \rangle = \frac{2}{3}, \quad \langle T_{i\gamma}^z T_{j\gamma}^z \rangle = 0. \quad (5.7)$$

Using these expectation values in Eq. (5.5) it follows,

$$\begin{aligned} J_{\text{MF}}^0 &= \frac{1}{3} J(1-\alpha) \left\{ \frac{3r_1 + r_2 + 2r_3}{9} - r_1 + r_2 \right\} \\ &+ \frac{1}{9} J\alpha \left\{ r_2 - r_1 + \frac{2r_2 + r_3}{3} \right\}, \end{aligned} \quad (5.8)$$

and one arrives at an analytic expression,

$$J_{\text{MF}}^0 = J(2-\alpha) \frac{-3r_1 + 5r_2 + r_3}{27}. \quad (5.9)$$

The classical exchange constant  $J_{\text{MF}}^0$  Eq. (5.9) is AF for small values of  $\eta$ , in agreement with the results presented in Secs. IIIB and IIIC, and changes sign at the critical value of Hund's exchange,

$$\eta_c = 0.188, \quad (5.10)$$



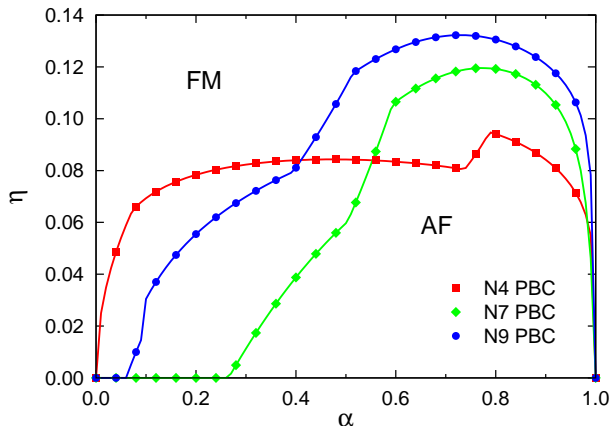


FIG. 14: (Color online) Phase diagrams obtained for disentangled spin-orbital interactions following Eq. (5.2) obtained for N4, N7 and N9 clusters with PBC. No intermediate phases were found between low-spin ( $\mathcal{S} = \mathcal{S}_{\min}$ ) and high-spin ( $\mathcal{S} = \mathcal{S}_{\max}$ ) phases.

where the present classical evaluation of the exchange constant predicts a transition to the FM phase. The present classical treatment suggests that this transition would occur simultaneously for all the bonds directly from the low-spin to high-spin state, with the maximal value of total spin  $\mathcal{S} = N/2$  for the cluster of  $N$  sites.

As usually, the MF Hamiltonian Eq. (5.2) implies a self-consistent solution of spin and orbital correlations. For instance, by solving a similar 1D problem within the MF approach self-consistently, one finds dimerization in FM spin-orbital chains at finite temperature.<sup>38</sup> Here we have applied the following iterative procedure for a system with spin and orbital interactions assumed to be isotropic on the triangular lattice: (i) for an initial value of spin scalar product  $\langle \vec{S}_i \cdot \vec{S}_j \rangle$  we solved the orbital Hamiltonian, next (ii) the effective exchange constants given by Eq. (5.4) were obtained, and (iii) they were used to determine the spin scalar product. This cycle was repeated until a self-consistent solution was found. We also used certain damping along the iteration process and enforced the symmetry of the considered clusters to accelerate the convergence as all the bonds are equivalent when PBC are used.

The phase diagrams obtained following the above MF procedure for the clusters N4, N7 and N9 with PBC are presented in Fig. 14. The applied procedure does not use the total spin symmetry, so intermediate (partial) spin polarization of the cluster could not be resolved. Since we solve here the effective spin Hamiltonian independently of the orbital problem, the total spin state is determined entirely by the sign of the exchange constant  $J_{\text{MF}}$ . The spin correlations were found to be either negative when  $J_{\text{MF}} > 0$ , indicating local AF (singlet-like) correlations, or were classical and FM, i.e.,  $\langle \vec{S}_i \cdot \vec{S}_j \rangle = +\frac{1}{4}$  when  $J_{\text{MF}} < 0$ . One finds that the low-spin states are

stable in a narrower range of the  $(\alpha, \eta)$  phase diagram for all three considered clusters, see Fig. 14, than when the exact diagonalization of the full Hamiltonian (2.3) is performed (shown in Fig. 13). In general, the phase boundary between the low-spin ( $\mathcal{S} = \mathcal{S}_{\min}$ ) and high-spin ( $\mathcal{S} = \mathcal{S}_{\max}$ ) phase was found at a lower value of  $\eta$  in each considered cluster than for the data extracted from exact diagonalization.

Moreover, the superexchange and direct exchange cases are rather special and FM states appear in these limits already for infinitesimal values of  $\eta$ . While the low-spin and high-spin state are degenerate in the direct exchange limit (at  $\alpha = 1$ ) for all three clusters shown in Fig. 14, in the superexchange case (at  $\alpha = 1$ ) such a degeneracy was found only for the N4 cluster. Both larger clusters N7 and N9 are FM already at  $\eta = 0$  in a range of small values of  $\alpha$ : for  $\alpha < 0.27$  in case of N7 and for  $\alpha < 0.05$  in case of N9 cluster. This behavior is surprising and suggests that the present MF procedure is unable to describe the present spin-orbital problem in a realistic way. We address this question in more detail in the next Sec. VB.

## B. Effective spin exchange constants

In a spin system, as the one obtained from the spin-orbital model, intersite spin correlations follow the sign of the exchange constant, i.e., when the exchange constant changes sign and becomes negative, the spins align in the FM phase. The spin model extracted in the MF approximation from the spin-orbital model Eq. (2.3) is given by

$$\mathcal{H}_s = J_{\text{MF}} \sum_{\langle ij \rangle} \vec{S}_i \cdot \vec{S}_j, \quad (5.11)$$

where the exchange constant is given by Eq. (5.4).

Let us consider now once again the N7 cluster as a representative case to contrast the results obtained from the exact diagonalization and the present MF approach. The low-spin phase has  $\mathcal{S} = 1/2$ , and the transition takes place to the  $\mathcal{S} = 7/2$  phase. Knowing that all the bonds are equivalent when PBC are used, and that each site has six neighbors, one finds that the spin correlation function for the low-spin  $\mathcal{S} = 1/2$  phase is  $\langle \vec{S}_i \cdot \vec{S}_j \rangle = -3/28$ , as deduced from Eq. (3.1). The phase diagram shown in Fig. 14 may be understood as following from the change of sign of the MF exchange constant Eq. (5.4). Indeed, when the effective exchange constant is obtained for the entire  $(\alpha, \eta)$  plane, the onset of FM phase corresponds to the line  $J_{\text{MF}} = 0$ , see Fig. 15(a). In general, the value of  $J_{\text{MF}}$  decreases with increasing  $\eta$  for any value of  $\alpha$ , but positive values of the effective exchange constant are found only in a range of  $\eta$  values, if  $0.27 < \alpha < 1$ . This situation is unusual as the effective superexchange obtained in the MF approach favors FM spin order, even in the absence of Hund's exchange. It could be understood

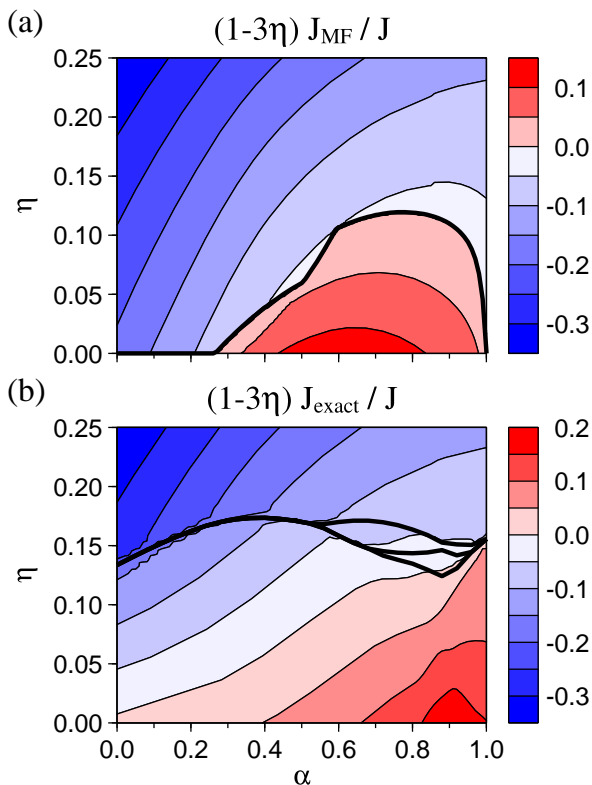


FIG. 15: (Color online) Contour plots of the effective exchange constant  $J_{\text{MF}}$  as obtained for N7 cluster with PBC from Eq. (5.4): (a) within the MF calculation which includes orbital fluctuations, and (b) using exact GS found in exact diagonalization. In case (a) the transition from low-spin to high-spin phase occurs when the exchange constant  $J_{\text{MF}}$  changes sign and becomes negative. Thick lines in (b) indicate the phase boundaries obtained between phases with increasing total spin value  $S = 1/2, 3/2, 5/2$  and  $7/2$  for increasing  $\eta$ .

as a consequence of strong orbital fluctuations in this regime which provide another mechanism of FM interactions playing an important role in the magnetic properties of the  $R\text{VO}_3$  perovskites ( $R=\text{La}, \text{Y}$ , etcetera).<sup>21,22</sup>

We remark that the phase diagram of N7 cluster (see Fig. 13) is quite different from the transition line shown in Fig. 15(a). Therefore, we conclude that the MF decoupling scheme does not capture the essential features of the joint spin-orbital dynamics which stabilizes the low-spin phase in a broad regime of parameters. Furthermore, the results shown in Fig. 15(b) prove that spin transition in the spin-orbital model is not related to the apparent sign change in the exchange constant  $J_{\text{MF}}$  Eq. (5.4) when it is calculated within the exact diagonalization approach. This also demonstrates that the frequently used MF procedure to extract the spin exchange constants<sup>23</sup> might lead to uncontrolled results, particularly for frustrated systems with disorder in a form of spin-orbital liquid.

Comparing the values of  $J_{\text{MF}}$  obtained using the MF procedure and the exact diagonalization [Figs. 15(a) and 15(b), respectively], a qualitative change is found for the

direct exchange case ( $\alpha = 1$ ), where positive values of  $J_{\text{MF}}$  extend now up to the transition point  $\eta \simeq 0.156$ . Also for lower values of  $\alpha$  the range of  $J_{\text{MF}} > 0$  is extended, particularly close to  $\alpha = 0$ . However, the value of  $\eta$  corresponding to  $J_{\text{MF}} = 0$  systematically decreases with decreasing  $\alpha$  and is as low as  $\tilde{\eta}_c \simeq 0.01$  at  $\alpha = 0$ . This behavior is in drastic contrast with the obtained transition from the low-spin to high-spin state, which occurs within the exact diagonalization method at a much higher value of  $\eta \simeq 0.16$  in the entire range of  $\alpha$ . Therefore, we conclude that the MF decoupling procedure given in Eq. (5.2) cannot be used in the present situation, similar as for the entangled states in the 1D spin-orbital chains with active  $t_{2g}$  orbitals.<sup>24</sup>

## VI. SUMMARY AND CONCLUSIONS

The present study unravels dimer correlations present in the spin-orbital model on the triangular lattice. By considering finite clusters with open boundary conditions we have shown that such dimer correlations do exist when the interactions are either of the superexchange or of the direct exchange type. When the symmetry of the lattice is broken by the boundary in triangular clusters, spin singlets are favored on bonds which originate from corner sites, and the orbital flavors adjust to the stronger channel, either to superexchange or to direct exchange. In fact, as different orbital states support these two types of magnetic interactions, the orbital distribution over the lattice is partly frustrated in the entire parameter regime, and this frustration contributes to the orbital disorder in the crossover regime, typically around  $\alpha = 0.6$ . The most striking result here is the collapse of valence-bond states in the intermediate regime and the onset of spin-orbital liquid. Such a disordered state realized already in finite clusters with open boundary conditions in the regime of competing interactions suggests that it could extend over a broader regime of parameters when the geometry would not favor particular way of symmetry breaking in the spin-orbital space.

Our study of the clusters with periodic boundary conditions provides indeed evidence that a quantum spin-orbital liquid phase is realized in the present  $d^1$  spin-orbital model designed for  $t_{2g}$  electrons on the geometrically frustrated triangular lattice. We would like to emphasize here that the frustrated lattice is necessary to remove tendency towards certain type of orbital order which could break the lattice symmetry in other cases, such as in the titanium or vanadium perovskites, and would support phases with long-range orbital accompanied by spin order of certain kind (usually following the Goodenough-Kanamori rules<sup>34</sup>). Thus, the spins behave here differently than in the spin model with Heisenberg interactions on the triangular lattice, and no spin order emerges when the spins couple to orbitals and both degrees of freedom undergo joint quantum fluctuations.

Although a mathematical proof is not possible, we pro-

vided, as we think, a rather complete and convincing evidence that the present  $d^1$  spin-orbital model realizes a paradigm of *spin-orbital liquid phase*, and the order-out-of-disorder mechanism does not apply when the Hilbert space contains coupled spin and orbital sectors. Previous search for this quantum state of matter in other systems, particularly in  $\text{LiNiO}_2$  where  $e_g$  orbitals are active on the triangular lattice,<sup>39</sup> were unsuccessful.<sup>40,41</sup> After considering the present model in more detail we suggest that the triple degeneracy of  $t_{2g}$  orbitals plays a crucial role in the onset of spin-orbital liquid, as the number of orbital flavors fits to the geometry of the triangular lattice. However, one might expect that instead a three-sublattice ordered state could arise, similar to the one known for spin system.<sup>3</sup> We argue that the coupling to the spins plays here a very important role and spin-orbital entanglement is a characteristic feature of the disordered state found in the absence of Hund's exchange (at  $J_H = 0$ ).

We have shown that both geometry and spin-orbital interactions are the origin of frustration in the model under consideration. One may wonder in this context whether *geometrical frustration* on the triangular lattice enhances *interaction frustration* for spin-orbital models. Quite generally, spin-orbital models contain in principle more channels which can be used for relieving enhanced frustration so one might still expect that some kind of ordered states would emerge. We argue that this problem is more subtle and its essence lies in the nature of spin-orbital entangled states. We have demonstrated by evaluating spin-orbital correlations that spin and orbital operators are entangled on the bonds and cannot be factorized. Under these circumstances important contributions to the ground state energy arise from joint spin-orbital fluctuations.

We have also found that Goodenough-Kanamori rules<sup>34</sup> are not obeyed by spin and orbital bond correlations in some cases. This concerns in particular the superexchange regime where the low-spin phase is stabilized by them. Such entangled states play an important role in the vanadium perovskites at finite temperature,<sup>21,22</sup> and lead to topological constraints on the hole motion which couples simultaneously to spin and optical excitation when states with entangled spin-orbital order are doped.<sup>42</sup> We emphasize that the spin-orbital entanglement occurs here on the bonds, and should not be confused with spin-orbital singlets arising from strong on-site spin-orbit coupling which leads to spin-orbital liquid with local singlets,<sup>43</sup> and might also generate exotic phases, as shown recently in the case of spin  $S = 1/2$  and a higher orbital quantum number (pseudospin)  $L = 1$ .<sup>44</sup>

By considering the magnetic transition to the ferromagnetic phase, we have shown that a likely scenario for

this transition is a crossover via the intermediate spin states before fully polarized ferromagnetic state sets in. This suggests that spin-orbital entangled states also play an important role in phases with partial spin polarization, stabilizing them in the regime of transition towards the fully polarized ferromagnetic phase. Moreover, we detected a general principle concerning the applicability of effective spin models derived from spin-orbital Hamiltonians. While this is a common practice nowadays which helps to understand and interpret the experimental data in systems with active orbital degrees of freedom,<sup>23</sup> we presented evidence that even in case when magnetic exchange constants can be accurately evaluated using the relevant orbital correlations, they might be inadequate to describe the magnetic ground state and excitations in such a system. This qualitative limitation could play a role particularly in disordered systems, where the physical consequences of entangled spin-orbital states are more severe.

In summary, the present spin-orbital model on the triangular lattice provides a beautiful example of highly frustrated interactions with the ground state dominated by: (i) quantum fluctuations, and (ii) spin-orbital entanglement. It is for this reason that several naive expectations which have their roots in classical expectations for complex spin systems do not apply, and it is even impossible to describe correctly the interactions for the magnetic degrees of freedom by decoupling them from the orbital ones. Although lattice distortions and coupling between the planes of a triangular lattice might destabilize the spin-orbital liquid found here, we hope that its experimental example could be established by future experimental studies. The spin-orbital disordered state provides a challenge both for the theory and for the experiment to find a way of describing magnetic excitations arising in a spin-orbital liquid phase.

### Acknowledgments

We thank George Jackeli, Bruce Normand and Karlo Penc for insightful discussions. J. C. thanks the Alexander von Humboldt Foundation for the fellowship during his stay at Max-Planck-Institut für Festkörperforschung, and acknowledges support by the Ministry of Education of Czech Republic under Grant No. MSM0021622410. A. M. O. acknowledges support by the Foundation for Polish Science (FNP) and by the Polish Ministry of Science and Higher Education under Project No. N202 069639.

---

<sup>1</sup> *Frustrated Spin Systems*, edited by H. T. Diep (World Scientific, Singapore, 2004).

<sup>2</sup> *Introduction to Frustrated Magnetism: Materials, Experiments, Theory*, edited by C. Lacroix, P. Mendels, and

- F. Mila, Springer Series in Solid-State Sciences, Vol. **164** (Springer, New York, 2011).
- <sup>3</sup> P. Fazekas, *Lectures on Electron Correlation and Magnetism* (World Scientific, Singapore, 1999).
  - <sup>4</sup> B. Normand, *Contemporary Phys.* **50**, 533 (2009).
  - <sup>5</sup> L. Balents, *Nature* **464**, 199 (2010).
  - <sup>6</sup> P. Fazekas and P. W. Anderson, *Philos. Mag.* **30**, 423 (1974).
  - <sup>7</sup> K. I. Kugel and D. I. Khomskii, *Usp. Fiz. Nauk* **136**, 621 (1982) [*Sov. Phys. Usp.* **25**, 231 (1982)]; C. Castellani, C. R. Natoli, and J. Ranninger, *Phys. Rev. B* **18**, 4945 (1978); **18**, 4967 (1978); **18**, 5001 (1978).
  - <sup>8</sup> G. Khaliullin, *Prog. Theor. Phys. Suppl.* **160**, 155 (2005); A. M. Oleś, *Acta Phys. Polon. A* **115**, 36 (2009).
  - <sup>9</sup> L. F. Feiner, A. M. Oleś, and J. Zaanen, *Phys. Rev. Lett.* **78**, 2799 (1997).
  - <sup>10</sup> D. I. Khomskii and M. V. Mostovoy, *J. Phys. A* **36**, 9197 (2003); Z. Nussinov, M. Biskup, L. Chayes, and J. van den Brink, *Europhys. Lett.* **67**, 990 (2004); B. Douçot, M. V. Feigel'man, L. B. Ioffe, and A. S. Ioselevich, *Phys. Rev. B* **71**, 024505 (2005).
  - <sup>11</sup> J. Dorier, F. Becca, and F. Mila, *Phys. Rev. B* **72**, 024448 (2005).
  - <sup>12</sup> S. Wenzel and W. Janke, *Phys. Rev. B* **78**, 064402 (2008); S. Wenzel, W. Janke, and A. M. Läuchli, *Phys. Rev. E* **81**, 066702 (2010).
  - <sup>13</sup> R. Orús, A. C. Doherty, and G. Vidal, *Phys. Rev. Lett.* **102**, 077203 (2009); L. Cincio, J. Dziarmaga, and A. M. Oleś, *Phys. Rev. B* **82**, 104416 (2010); F. Trouselet, A. M. Oleś, and P. Horsch, *EPL* **91**, 40005 (2010).
  - <sup>14</sup> W. Brzezicki, J. Dziarmaga, and A. M. Oleś, *Phys. Rev. B* **75**, 134415 (2007); E. Eriksson and H. Johannesson, *ibid.* **79**, 224424 (2009); W. Brzezicki and A. M. Oleś, *ibid.* **80**, 014405 (2009).
  - <sup>15</sup> W. Brzezicki and A. M. Oleś, *Phys. Rev. B* **82**, 060401 (2010).
  - <sup>16</sup> L. F. Feiner and A. M. Oleś, *Phys. Rev. B* **59**, 3295 (1999); A. M. Oleś, L. F. Feiner, and J. Zaanen, *ibid.* **61**, 6257 (2000).
  - <sup>17</sup> M. Daghofer, W. von der Linden, and A. M. Oleś, *Phys. Rev. B* **70**, 184430 (2004).
  - <sup>18</sup> M. Daghofer, A. M. Oleś, D. M. Neuber, and W. von der Linden, *Phys. Rev. B* **73**, 104451 (2006).
  - <sup>19</sup> J. van der Brink, P. Horsch, F. Mack, and A. M. Oleś, *Phys. Rev. B* **59**, 6795 (1999); L. F. Feiner and A. M. Oleś, *ibid.* **71**, 144422 (2005).
  - <sup>20</sup> G. Khaliullin and S. Maekawa, *Phys. Rev. Lett.* **85**, 3950 (2000); G. Khaliullin, *Phys. Rev. B* **64**, 212405 (2001).
  - <sup>21</sup> G. Khaliullin, P. Horsch, and A. M. Oleś, *Phys. Rev. Lett.* **86**, 3879 (2001); *Phys. Rev. B* **70**, 195103 (2004); A. M. Oleś, P. Horsch, and G. Khaliullin, *ibid.* **75**, 184434 (2007).
  - <sup>22</sup> P. Horsch, A. M. Oleś, L. F. Feiner, and G. Khaliullin, *Phys. Rev. Lett.* **100**, 167205 (2008).
  - <sup>23</sup> A. M. Oleś, P. Horsch, G. Khaliullin, and L. F. Feiner, *Phys. Rev. B* **72**, 214431 (2005).
  - <sup>24</sup> A. M. Oleś, P. Horsch, L. F. Feiner, and G. Khaliullin, *Phys. Rev. Lett.* **96**, 147205 (2006).
  - <sup>25</sup> B. Normand and A. M. Oleś, *Phys. Rev. B* **78**, 094427 (2008).
  - <sup>26</sup> G. Jackeli and D. A. Ivanov, *Phys. Rev. B* **76**, 132407 (2007).
  - <sup>27</sup> H. F. Pen, J. van den Brink, D. I. Khomskii, and G. A. Sawatzky, *Phys. Rev. Lett.* **78**, 1323 (1997).
  - <sup>28</sup> J. Zaanen and A. M. Oleś, *Phys. Rev. B* **48**, 7197 (1993).
  - <sup>29</sup> W. Koshibae and S. Maekawa, *Phys. Rev. Lett.* **91**, 257003 (2003); G. Khaliullin, W. Koshibae, and S. Maekawa, *ibid.* **93**, 176401 (2004).
  - <sup>30</sup> A. M. Oleś, *Phys. Rev. B* **28**, 327 (1983).
  - <sup>31</sup> J. S. Griffith, *The Theory of Transition Metal Ions* (Cambridge University Press, Cambridge, 1971).
  - <sup>32</sup> J. Zaanen and G. A. Sawatzky, *J. Solid State Chem.* **88**, 8 (1990).
  - <sup>33</sup> B. Frischmuth, F. Mila, and M. Troyer, *Phys. Rev. Lett.* **82**, 835 (1999); F. Mila, B. Frischmuth, A. Deppeler, and M. Troyer, *ibid.* **82**, 3697 (1999).
  - <sup>34</sup> J. B. Goodenough, *Magnetism and the Chemical Bond* (Interscience, New York, 1963); J. Kanamori, *J. Phys. Chem. Solids* **10**, 87 (1959).
  - <sup>35</sup> The transition line obtained for N3 cluster corrects the phase diagram given in Fig. 13 of Ref. 25.
  - <sup>36</sup> The transition line obtained for N4 cluster corrects the phase diagram given in Fig. 16 of Ref. 25.
  - <sup>37</sup> N. N. Kovaleva, A. M. Oleś, A. M. Balbashov, A. Maljuk, D. N. Argyriou, G. Khaliullin, and B. Keimer, *Phys. Rev. B* **81**, 235130 (2010).
  - <sup>38</sup> J. Sirker, A. Herzog, A. M. Oleś, and P. Horsch, *Phys. Rev. Lett.* **101**, 157204 (2008); A. Herzog, P. Horsch, A. M. Oleś, and J. Sirker, *J. Phys.: Conf. Series* **200**, 022017 (2010).
  - <sup>39</sup> F. Vernay, K. Penc, P. Fazekas, and F. Mila, *Phys. Rev. B* **70**, 014428 (2004); F. Vernay, A. Ralko, F. Becca, and F. Mila, *ibid.* **74**, 054402 (2006); F. Mila, F. Vernay, A. Ralko, F. Becca, P. Fazekas, and K. Penc, *J. Phys.: Condens. Matter* **19**, 145201 (2007).
  - <sup>40</sup> M. V. Mostovoy and D. I. Khomskii, *Phys. Rev. Lett.* **89**, 227203 (2002).
  - <sup>41</sup> A. Reitsma, L. F. Feiner, and A. M. Oleś, *New J. Phys.* **7**, 121 (2005).
  - <sup>42</sup> K. Wohlfeld, A. M. Oleś, and P. Horsch, *Phys. Rev. B* **79**, 224433 (2009).
  - <sup>43</sup> G. Chen, L. Balents, and A. P. Schnyder, *Phys. Rev. Lett.* **102**, 096406 (2009); G. Chen, A. P. Schnyder, and L. Balents, *Phys. Rev. B* **80**, 224409 (2009).
  - <sup>44</sup> G. Jackeli and G. Khaliullin, *Phys. Rev. Lett.* **102**, 017205 (2009); **103**, 067205 (2009).